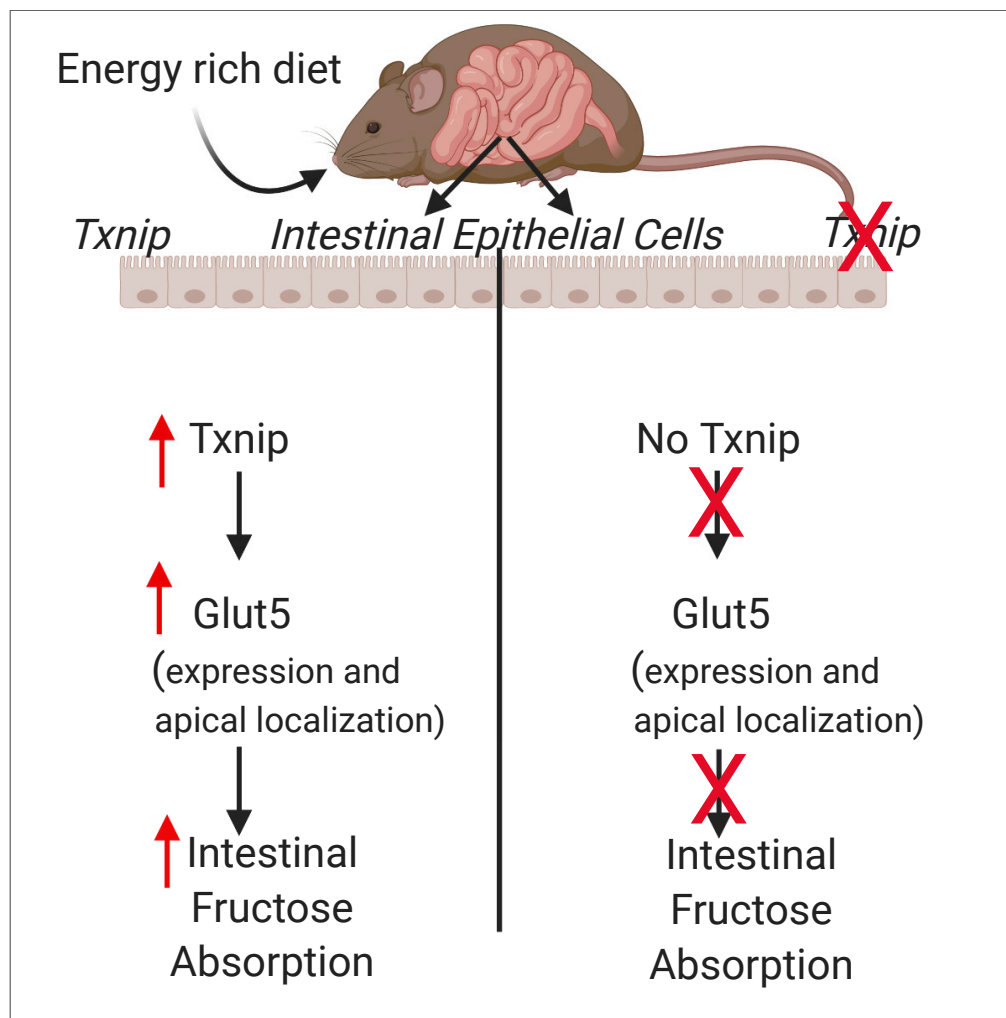


Article

Thioredoxin Interacting Protein Is Required for a Chronic Energy-Rich Diet to Promote Intestinal Fructose Absorption



Anu Shah, Sezin Dagdeviren, Jordan P. Lewandowski, ..., Amy J. Wagers, Roy J. Soberman, Richard T. Lee

richard_lee@harvard.edu

HIGHLIGHTS

Consumption of energy-rich diets (ERDs) promotes intestinal fructose absorption

Intestinal Txnip is required for increased fructose absorption by ERD

Txnip increases fructose transporter Glut5 protein and gene expression

Txnip forms a complex with Rab11a to facilitate the apical localization of Glut5

Shah et al., iScience 23, 101521
September 25, 2020 © 2020
The Author(s).
<https://doi.org/10.1016/j.isci.2020.101521>

Article

Thioredoxin Interacting Protein Is Required for a Chronic Energy-Rich Diet to Promote Intestinal Fructose Absorption

Anu Shah,¹ Sezin Dagdeviren,¹ Jordan P. Lewandowski,¹ Angela B. Schmider,² Elisabeth M. Ricci-Blair,¹ Niranjana Natarajan,¹ Henna Hundal,¹ Hye Lim Noh,³ Randall H. Friedline,³ Charles Vidoudez,⁵ Jason K. Kim,^{3,4} Amy J. Wagers,^{1,6,7} Roy J. Soberman,² and Richard T. Lee^{1,8,9,*}

SUMMARY

Increased consumption of fats and added sugars has been associated with an increase in metabolic syndromes. Here we show that mice chronically fed an energy-rich diet (ERD) with high fat and moderate sucrose have enhanced the absorption of a gastrointestinal fructose load, and this required expression of the arrestin domain protein Txnip in the intestinal epithelial cells. ERD feeding induced gene and protein expression of Glut5, and this required the expression of Txnip. Furthermore, Txnip interacted with Rab11a, a small GTPase that facilitates the apical localization of Glut5. We also demonstrate that ERD promoted Txnip/Glut5 complexes in the apical intestinal epithelial cell. Our findings demonstrate that ERD facilitates fructose absorption through a Txnip-dependent mechanism in the intestinal epithelial cell, suggesting that increased fructose absorption could potentially provide a mechanism for worsening of metabolic syndromes in the setting of a chronic ERD.

INTRODUCTION

The consumption of energy-dense diets or the “western diet” has coincided with an increase in metabolic diseases including obesity and type 2 diabetes (Chatterjee et al., 2017). An increase in “added sugars,” particularly in liquid forms such as in sugar-sweetened beverages, has also been associated with an increase in metabolic diseases (Bray et al., 2004; Khan and Sievenpiper, 2016; Schwarz et al., 2017). Sucrose, or table sugar, is composed of one molecule of fructose and one molecule of glucose. Although they are isomers, fructose metabolism differs from glucose metabolism as fructose can readily be diverted to the liver into a *de novo lipogenesis* pathway (Lyssiotis and Cantley, 2013). Recent evidence suggests that fructose consumption at low doses may simply be providing more glucose, as intestinal cells can metabolize low doses of fructose into glucose (Jang et al., 2018). However, at higher doses, fructose may be absorbed rapidly into the liver, bypassing key regulatory steps in glycolysis, and thereby stimulating hepatic fat synthesis (Jang et al., 2018).

Txnip, a member of arrestin domain-containing protein family (Patwari and Lee, 2012), is a multifunctional intracellular protein that coordinates signaling pathways, including oxidative stress, endoplasmic reticulum stress, apoptosis, DNA damage, and inflammation (Spindel et al., 2011). The function of Txnip has been defined through *in vivo* studies as a regulator of carbohydrate metabolism (Chutkow et al., 2008; Parikh et al., 2007; Waldhart et al., 2017). Txnip regulates glucose metabolism (Parikh et al., 2007) by binding to glucose transporters, Glut1 and Glut4 (Waldhart et al., 2017; Wu et al., 2013). Txnip can also regulate fructose metabolism in the setting of severe streptozotocin-induced diabetes (Dotimas et al., 2016), possibly through binding to fructose transporters, Glut5 and Glut2, in intestinal epithelial cells. Previous epidemiological studies have demonstrated the association of fructose consumption with type 2 diabetes (Malik et al., 2010; Tappy and Le, 2010). Thus, to explore the relationship of an energy-rich diet (ERD) and fructose metabolism, we studied acute fructose absorption in mice fed with an ERD.

RESULTS AND DISCUSSION

Energy-Rich Diet Promotes Fructose Absorption and Elevates Txnip Expression

As hyperglycemia increases Txnip expression significantly (Dotimas et al., 2016), we studied normoglycemic mice fed with an ERD, generally called a high-fat diet (HFD); this diet includes 7% calories as sucrose or 3.5%

¹Department of Stem Cell and Regenerative Biology and the Harvard Stem Cell Institute, Harvard University, Sherman Fairchild Biochemistry Building, 7 Divinity Avenue, Cambridge, MA 02138, USA

²Molecular Imaging Core and Nephrology Division, Department of Medicine, Massachusetts General Hospital, Charlestown, MA 02129, USA

³Program in Molecular Medicine, Department of Medicine, University of Massachusetts Medical School, Worcester, MA 01605, USA

⁴Division of Endocrinology, Metabolism and Diabetes, Department of Medicine, University of Massachusetts Medical School, Worcester, MA 01605, USA

⁵Small Molecule Mass Spectrometry, Harvard University, Cambridge, MA 02138, USA

⁶Glenn Center for the Biology of Aging, Harvard Medical School, Boston, MA 02115, USA

⁷Section on Islet Cell and Regenerative Biology, Joslin Diabetes Center, Boston, MA 02215, USA

⁸Cardiovascular Division, Department of Medicine, Brigham and Women's Hospital and Harvard Medical School, Boston, MA 02115, USA

⁹Lead Contact

*Correspondence: richard_lee@harvard.edu
<https://doi.org/10.1016/j.isci.2020.101521>



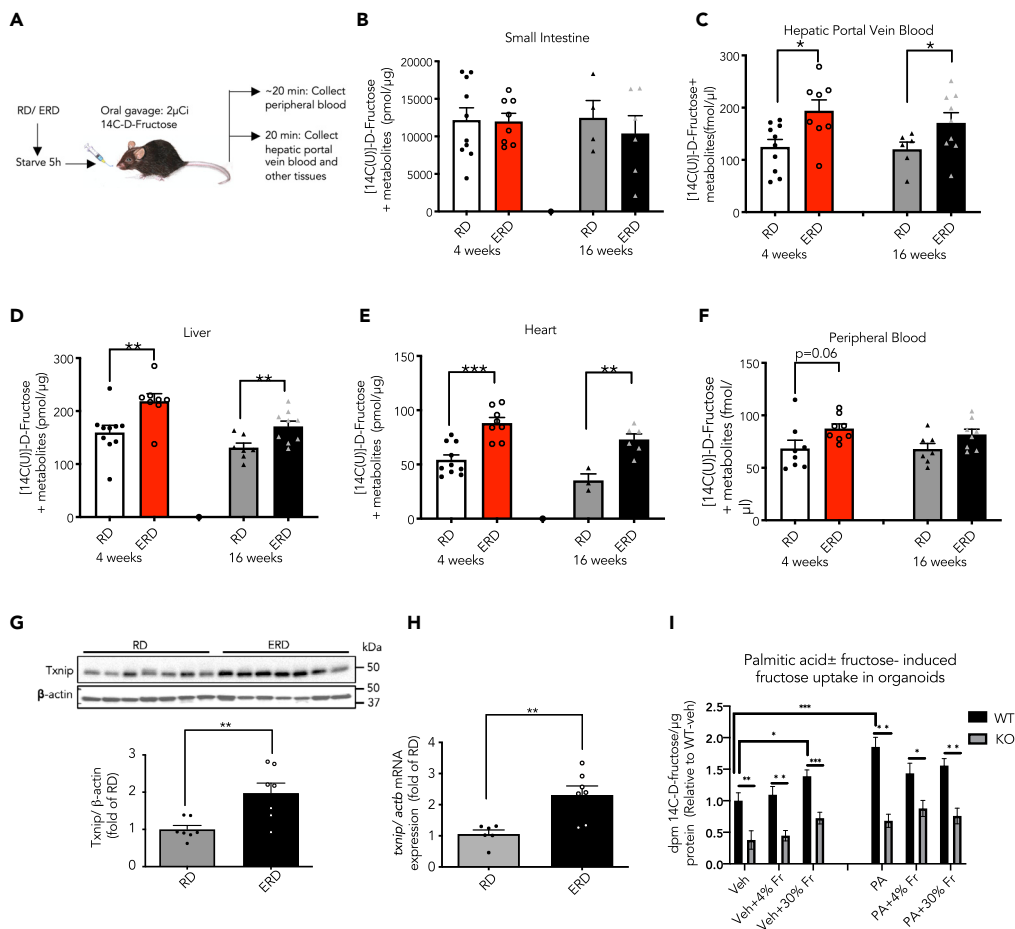


Figure 1. Energy-Rich Diet Promotes Fructose Absorption and Elevates Txnip Expression

(A) Schematic representation of the experimental procedure.

(B–F) Fructose absorption (i.e., ^{14}C -fructose + metabolites) by various tissues from 4 weeks ($n = 7\text{--}8$) and 16 weeks ($n = 3\text{--}8$) RD/ERD diet-fed mice after the intragastric oral gavage of ^{14}C -fructose. Values are shown as mean \pm SEM. * $p < 0.05$, ** $p < 0.01$, or *** $p < 0.001$ as calculated by unpaired t test.

(G) A representative western blot and quantitative analysis of Txnip (molecular weight: 50kDa) and β -actin (loading control, molecular weight: 42kDa) in the jejunal lysates of RD/ERD-fed mice ($n = 7$ mice/diet). Values are shown as mean \pm SEM. ** $p < 0.01$ as calculated by unpaired t test.

(H) Gene expression of *Txnip* normalized to *actb*, house-keeping gene, in the jejunal samples from RD/ERD-fed mice ($n = 6\text{--}7$ mice/diet). Values are shown as mean \pm SEM. ** $p < 0.01$ as calculated by unpaired t test.

(I) Intestinal uptake of fructose was performed in the intestinal organoids extracted from Txnip wild-type (WT) and knockout (KO) mice. Both palmitic acid (PA) and 30% fructose (veh+30% Fr) significantly increased fructose uptake in WT organoids when compared with WT-veh. However, the deletion of *Txnip* significantly reduced both fructose-induced and PA-induced fructose uptake. There was no significant increase in the PA-induced fructose uptake by Txnip WT organoids after the addition of either 4% Fr or 30% Fr ($n = 7\text{--}8$ wells).

Values are shown as mean \pm SEM. * $p < 0.05$, ** $p < 0.01$, or *** $p < 0.001$ as calculated by unpaired t test. WT, wild-type; KO, knockout; veh, vehicle/BSA; PA, palmitic acid; and Fr, fructose.

See also [Tables S1](#) and [S2](#) and [Figures S1](#) and [S2](#).

calories as fructose. C57Bl/6J male mice at ages 7–9 weeks were placed on RD (regular diet) or ERD for 4 or 16 weeks and their metabolic profiles ([Table S1](#)) were obtained. As seen in [Tables S1](#) and [S2](#), the fasting blood glucose levels did not change with ERD feeding, suggesting that fasting blood glucose levels did not influence the differences in fructose absorption in our study. As outlined in the experimental procedures ([Figure 1A](#)), the mice were then administered 2 μCi of radiolabeled [^{14}C -(U)]-D fructose dissolved in 1:1 fructose mannitol solution using intragastric gavage to examine intestinal fructose absorption. Although fructose is generally consumed together with glucose, our data indicate that ERD increases acute fructose absorption in the presence of either glucose or mannitol in the gavage solution ([Figure S1A](#)). We assayed tissues at 20 min after gavage as

this is the peak time for fructose absorption in normal and diabetic mice (Dotimas et al., 2016). There was no difference in the isotope retained in the small intestine, which includes both luminal and absorbed fructose (Figure 1B); but interestingly, in both the short- (4 weeks) and long-term (16 weeks) ERD-fed mice, the amount of absorbed isotope from gastrointestinal fructose was significantly increased in the portal vein, liver, and heart, as depicted in Figures 1C–1E. Furthermore, a trend for increased ^{14}C -fructose + metabolites (hereafter termed only as ^{14}C -fructose) level in the peripheral blood of ERD mice versus RD mice was also observed, consistent with the known first-pass effect of fructose by the liver (Lyssiotis and Cantley, 2013) (Figure 1F). Our acute bolus fructose dose of approximately 1.0 g/kg was on the same order as most of the experiments performed by Jang et al. (Jang et al., 2018) in their study. We did not measure the amount of fructose transmitted to the colon in our study due to the early times of sacrifice (20 min versus 60–120 min in the experiments by Jang et al., 2018) required to access the portal vein, but it is possible that it would differ in the setting of ERD or added fructose to drinking water. Collectively, these data indicate that ERD feeding increased fructose absorption from small intestine via the hepatic portal vein.

Consistent with increased hepatic Txnip protein expression previously reported in HFD/ERD-fed mice (Shao et al., 2012), the jejunum from the ERD-fed mice had a significant increase in Txnip protein (Figure 1G and 2.0 ± 0.3 -fold, $p < 0.01$) and *Txnip* gene (Figure 1H and 2.3 ± 0.3 -fold, $p < 0.01$) expressions when compared with the RD-fed mice. These data show that ERD feeding promotes fructose absorption and Txnip expression in the jejunum. To determine if the absorbed gastrointestinal fructose load remained in the form of fructose in the intestinal epithelial cell, a mass spectrometry-based analysis was performed using [^{13}C]-fructose using an identical protocol as that described in the previous paragraph for experiments with [^{14}C -(U)]-D fructose. The intestine contained primarily ^{13}C -labeled fructose and a small amount of isotope-labeled glucose metabolite (labeled fructose 391.89 ± 37.60 nmol/mg tissue versus 0.48 ± 0.33 nmol/mg tissue, $n = 10$ mice, $***p < 0.001$ versus labeled glucose), consistent with recently published results with high fructose influx (Jang et al., 2018). Of note, when compared with RD-fed mice, ERD-fed villin cre mice showed a trend of increased ^{13}C -fructose-1-phosphate in the jejunum (Figure S1B).

We also determined the impact of chronic fructose consumption on fructose absorption. For this, we conducted a 4-week-long study wherein we placed C57BL/6J mice on an RD or ERD with and without 30% fructose solution in drinking water, as described previously (Softic et al., 2017). Mice on RD and *ad libitum* access to water were used as the control group. As illustrated in Figure S2C, there was an increase in acute fructose uptake with chronic consumption of fructose in drinking water, irrespective of the diet consumed. In addition, fructose in drinking water accelerated the time to peak fructose absorption from 20 min to 10 min, although the differences between groups were qualitatively similar. We speculate that there could be an evolutionary advantage as to why ERD feeding promotes fructose absorption. ERD may lead to an inflammatory state, and in this setting, adaptation to harness more calories could be beneficial. This concept is similar to a theory of insulin resistance suggested for HFD and type 2 diabetes (Soeters and Soeters, 2012).

To further explore our *in vivo* finding, we extracted intestinal organoids from Txnip wild-type (WT) and knockout (KO) mice to assess fructose absorption according to a protocol described previously (Zietek et al., 2015). As illustrated in Figure 1I, we subjected the intestinal organoids to an “energy-rich environment” using 50 μM palmitic acid (PA) or BSA (vehicle) as previously reported for the intestinal organoids (Beyaz et al., 2016), as well as added either 4% (approximating the percentage of fructose in the ResearchDiets Inc. High Fat Diet, D12492) or 30% fructose to the solution for 3 h. Interestingly, as shown in Figure 1I, there was a significant increase in fructose uptake by the PA-treated WT organoids ($p < 0.001$ versus WT-vehicle) and 30% fructose-treated WT organoids ($p < 0.05$ versus WT-vehicle). However, there was no significant difference between PA-treated groups after the addition of 4% fructose ($p = 0.08$ versus PA alone) or 30% fructose ($p = 0.1$ versus PA alone). We also found that exogenous fructose alone significantly increased fructose uptake in the WT versus Txnip KO organoids ($p < 0.001$), indicating that Txnip is crucial for fructose-induced acute fructose absorption by organoids. Overall, when compared with ERD, the data from Figure S2 suggest that fructose in drinking water has a larger impact on fructose absorption than ERD. We have previously demonstrated that fructose in drinking water promoted fructose absorption in intestinal epithelial cells, and for this, Txnip was necessary (Dotimas et al., 2016). Thus, in the current study, we sought to explore the effect of ERD on fructose absorption.

Deletion of *Txnip* in the Intestinal Epithelial Cells Mitigates ERD-Induced Fructose Absorption

Next, we explored *in vivo* if Txnip is an essential component of ERD-induced fructose absorption. As a majority of the fructose is absorbed by the proximal part of the small intestine via intestinal epithelial cells

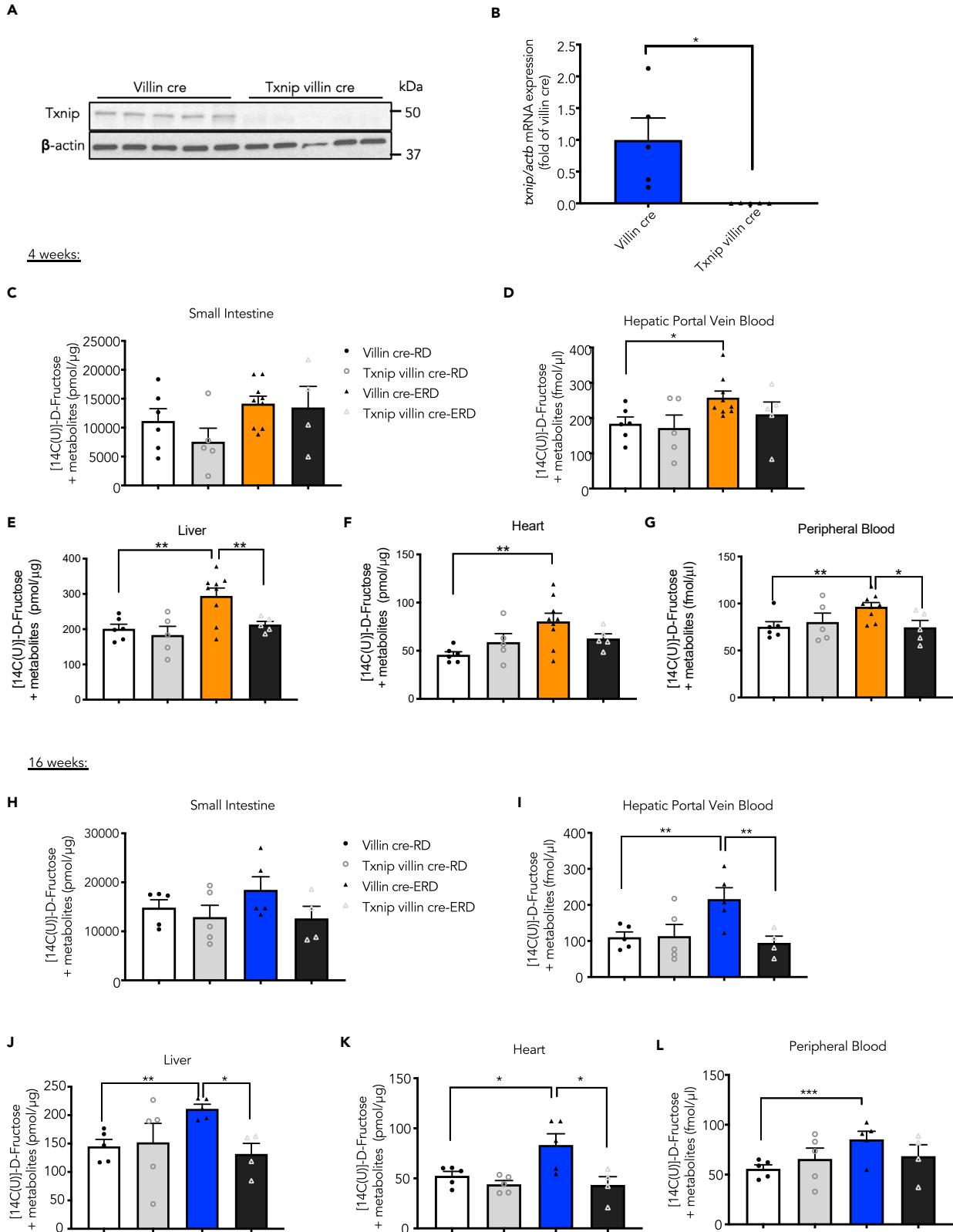


Figure 2. Deletion of *Txnip* in the Intestinal Epithelial Cells Mitigates ERD-Induced Fructose Absorption

(A) A representative western blot demonstrating successful abolition of *Txnip* in the villi of *Txnip* villin cre mice (n = 5).

(B) Gene expression of *Txnip* normalized to *actb* in villi from villin cre and *Txnip* villin cre mice (n = 5). Values are shown as mean \pm SEM. *p < 0.05 as calculated by unpaired t test.

(C–L) (C–G) Fructose absorption (i.e., ^{14}C -fructose + metabolites) by various tissues from 4 weeks (n = 4–8) and (H–L) 16 weeks (n = 4–5) in RD/ERD-fed mice after the oral gavage of ^{14}C -fructose.

Values are shown as mean \pm SEM. *p < 0.05, **p < 0.01, or ***p < 0.001 as calculated by unpaired t test.

See also [Table S2](#).

(Bray et al., 2004), we studied mice with genetic deletion of *Txnip* in intestinal epithelial cells by crossing *Txnip*^{fl^{ox}/fl^{ox}} (*Txnip*^{fl/fl}) mice with villin cre mice. We confirmed *Txnip* deletion in the villi of *Txnip*^{fl/fl} villin cre^{+/-} (hereafter called *Txnip* villin cre) mice when compared with the villi of villin cre-controls (*Txnip*^{+/+} villin cre^{+/-}, hereafter called villin cre) by both western analysis and qRT-PCR (Figures 2A and 2B). Moreover, unlike systemic *Txnip*-KO mice (Chutkow et al., 2008), the metabolic profiles displayed by the *Txnip* villin cre mice were similar to those of the villin cre mice (Tables S1 and S2), implying that the experimental outcomes were due to the intestinal epithelium deletion of *Txnip* and not due to the global metabolic effects of *Txnip* deletion. Also, note that insulin levels were increased by the ERD as anticipated (Table 1), and this could influence transport of isotope from fructose into the liver and heart. Interestingly, from the metabolic studies performed, the only differences noted between the ERD-fed *Txnip* villin cre mice and villin-cre controls on the same diet were in their total food consumption (1.6 \pm 0.2-fold versus ERD-fed villin cre, n = 4, p < 0.05) and energy expenditure (ERD-fed *Txnip* villin cre versus ERD-fed villin cre (kcal/h/kg): 22.5 \pm 0.3 versus 21.3 \pm 0.3, n = 4, p < 0.05), which were higher in the ERD-fed *Txnip* villin cre mice (Table 1).

We then randomized a second cohort of 7- to 9-week-old *Txnip* villin cre and villin cre mice to RD versus ERD for short-term (4 weeks, Figures 2C–2G) or long-term (16 weeks, Figures 2H–2L) experiments and assessed fructose absorption. By 4 weeks of ERD feeding, consistent with aforementioned data on RD/ERD-fed C57Bl/6J mice, we found a significant increase in fructose absorption into the hepatic portal vein, liver, heart, and peripheral blood in the villin cre mice (Figures 2D–2G). In contrast, we did not observe increased uptake of the isotope in the livers of the ERD-fed *Txnip* villin cre mice, where *Txnip* was absent in the intestinal epithelium. The impact of deletion of *Txnip* in intestinal epithelial cells was even more pronounced in the *Txnip* villin cre mice that were placed on ERD for 16 weeks when compared with villin cre mice placed on the same diet, with significant reductions in isotope uptake in the hepatic portal vein, liver, and heart (Figures 2I–2L). These findings were supported by the fructose uptake experiments performed on intestinal organoids (Figure 1I), wherein we showed that deletion of *Txnip* significantly mitigated fructose absorption (p < 0.01 for WT-vehicle versus KO-vehicle). Moreover, despite the presence of PA, *Txnip* KO organoids failed to show enhanced fructose uptake (p < 0.001 versus *Txnip* WT-PA). The data are consistent with the hypothesis that *Txnip* is required for a chronic ERD to promote intestinal fructose absorption. Collectively, although basal level of *Txnip* is adequate to drive physiological/normal fructose absorption, an increased *Txnip* expression stimulated by ERD is necessary for ERD-induced fructose absorption.

***Txnip* Is Required for the Energy-Rich Diet-Induced *Glut5* Expression**

We next explored the mechanism for increased fructose absorption by *Txnip* under an ERD. Although a reciprocal association between *Txnip* and tissue responsiveness to nitric oxide has been reported before (Sverdllov et al., 2013), we examined the changes in NO levels in intestinal lysates obtained from villin cre and *Txnip* villin cre mice on RD/ERD to investigate whether NO may be responsible for the difference observed in fructose absorption and thus serve as a potential mechanism. As seen in Figure S3, the presence or absence of *Txnip* in the intestinal mucosal lysates did not appear to have a substantial role in regulating parameters of nitric oxide effect. Next, we assessed the expression of *Glut2* and *Glut5*, the fructose transporters in the intestine, in the intestinal mucosa from these mice. We performed gene expression of *Glut2* (*Slc2a2*) in the jejunal tissues, and there were no significant differences in the gene expression of *Glut2* with diets and/or deletion of *Txnip* in epithelial cells (n = 4 animals per group). Interestingly, we observed a significant increase in the *Slc2a5* gene (2.5 \pm 0.5-fold versus villin cre RD, n = 3–4, p < 0.05) and *Glut5* protein (7.6 \pm 1.4-fold versus villin cre RD, n = 4, p < 0.001, double bands) (Figures 3A and 3B) with ERD feeding. Deletion of *Txnip* in the intestinal epithelium dramatically reduced *Glut5* gene and protein expression under ERD feeding (Figures 3A and 3B). These findings reveal that *Txnip* is essential for ERD-induced *Glut5* expression in the intestine.

Metabolic Parameters	Villin Cre		Txnip Villin Cre	
	RD (n = 4)	ERD (n = 4)	RD (n = 4)	ERD (n = 4)
Fat mass (g)	2.9 ± 0.5	19.5 ± 0.5	2.4 ± 0.4	17.3 ± 1.9
Lean mass (g)	26.0 ± 1.3	27.2 ± 0.9	24.9 ± 1.4	25.8 ± 1.4
Body weight (g)	30.4 ± 1.4	47.7 ± 0.5	28.7 ± 1.3	43.8 ± 3.2
AUC (ipGTT)	17,132 ± 918	24,707 ± 1,858	17,070 ± 2,193	26,256 ± 2,919
24-h food intake(kcal)	12.5 ± 0.6	5.2 ± 0.5	11.8 ± 0.6	8.3 ± 1.0*
24-h water intake (mL)	3.4 ± 0.2	0.8 ± 0.2	3.2 ± 0.3	1.5 ± 0.2*
VO ₂ consumption rate (mL/h/kg)	4,110 ± 74	4,466 ± 69	4,050 ± 70	4,700 ± 71*
VCO ₂ production rate (mL/h/kg)	3,673 ± 62	3,347 ± 56	3,661 ± 68	3,599 ± 58**
Energy expenditure rate (kcal/h/kg)	20.3 ± 0.4	21.3 ± 0.3	20.0 ± 0.3	22.5 ± 0.3*
Respiratory exchange ratio	0.9 ± 0.0	0.7 ± 0.0	0.9 ± 0.0	0.8 ± 0.0**
Total physical activity (counts/h)	6,958 ± 475	2,722 ± 360	4,653 ± 337***	3,245 ± 188
Liver triglycerides (μmol/g)	12.8 ± 1.7	18.3 ± 4.6	11.8 ± 2.4	22.1 ± 6.0
Plasma cholesterol (mg/dL)	81 ± 2.0	210 ± 15.0	78 ± 3.0	198 ± 14.0
HDL (mg/dL)	71 ± 2.0	172 ± 12.0	68 ± 3.0	155 ± 4.0
LDL (mg/dL)	74 ± 3.0	172 ± 6.0	68 ± 4.0	170 ± 17.0
Insulin (ng/mL)	0.56 ± 0.2 (n = 5)	2.2 ± 0.5 [#] (n = 4)	0.56 ± 0.1 (n = 5)	2.7 ± 0.5 ^{##} (n = 4)

Table 1. Metabolic Outcomes from Villin Cre and Txnip Villin Cre Mice

AUC, area under the curve; HDL, high-density lipoprotein; ipGTT, intraperitoneal glucose tolerance test; LDL, low-density lipoprotein;

Results are expressed as mean ± SEM (n=4 mice/ group).

p values were calculated using an unpaired Student's t test. *p<0.05, **p<0.01, and ***p<0.001 versus villin cre with the same diet; # p<0.05, ##p<0.01 versus RD-fed mice from the same strain.

Recently, it was reported that carbohydrate responsive element-binding protein (ChREBP) bound directly to *Slc2a5* (Kim et al., 2017) in the intestine. As Txnip promotes the de-phosphorylation and nuclear translocation of ChREBP (Chen et al., 2014), we hypothesized that ERD-induced Txnip would enhance the binding of ChREBP to the promoter region of *Slc2a5*. To test for this possible mechanism, we performed ChREBP chromatin immunoprecipitation (ChIP)-qPCR on intestinal samples from mice that were fed either an RD or ERD and also confirmed that the ChREBP ChIP assay responded to classical stimuli (Figure S4). We assayed previously reported ChREBP-binding sites in the thioredoxin-interacting protein (*Txnip*) (Poungvarin et al., 2015) and pyruvate kinase L/R (*Pklr*) promoter regions (Kim et al., 2017), including observing changes in their gene expressions after challenging with ERD (Figure S4C). At the *Txnip* and *Pklr* promoter regions, we found an enrichment of H3K4me3, therefore indicating an active promoter (Figures 3C and 3D, top panel). We also found enrichment for ChREBP at the *Txnip* (r1) and *Pklr* (r2) promoters in both RD and ERD samples when compared with control IgG samples as well as compared with a previously reported ChREBP-negative control region (Kim et al., 2017) (Figures 3C and 3D). We noted that a previous ChREBP-binding region in the *Slc2a5* locus (Kim et al., 2017) suggested to be the promoter contains

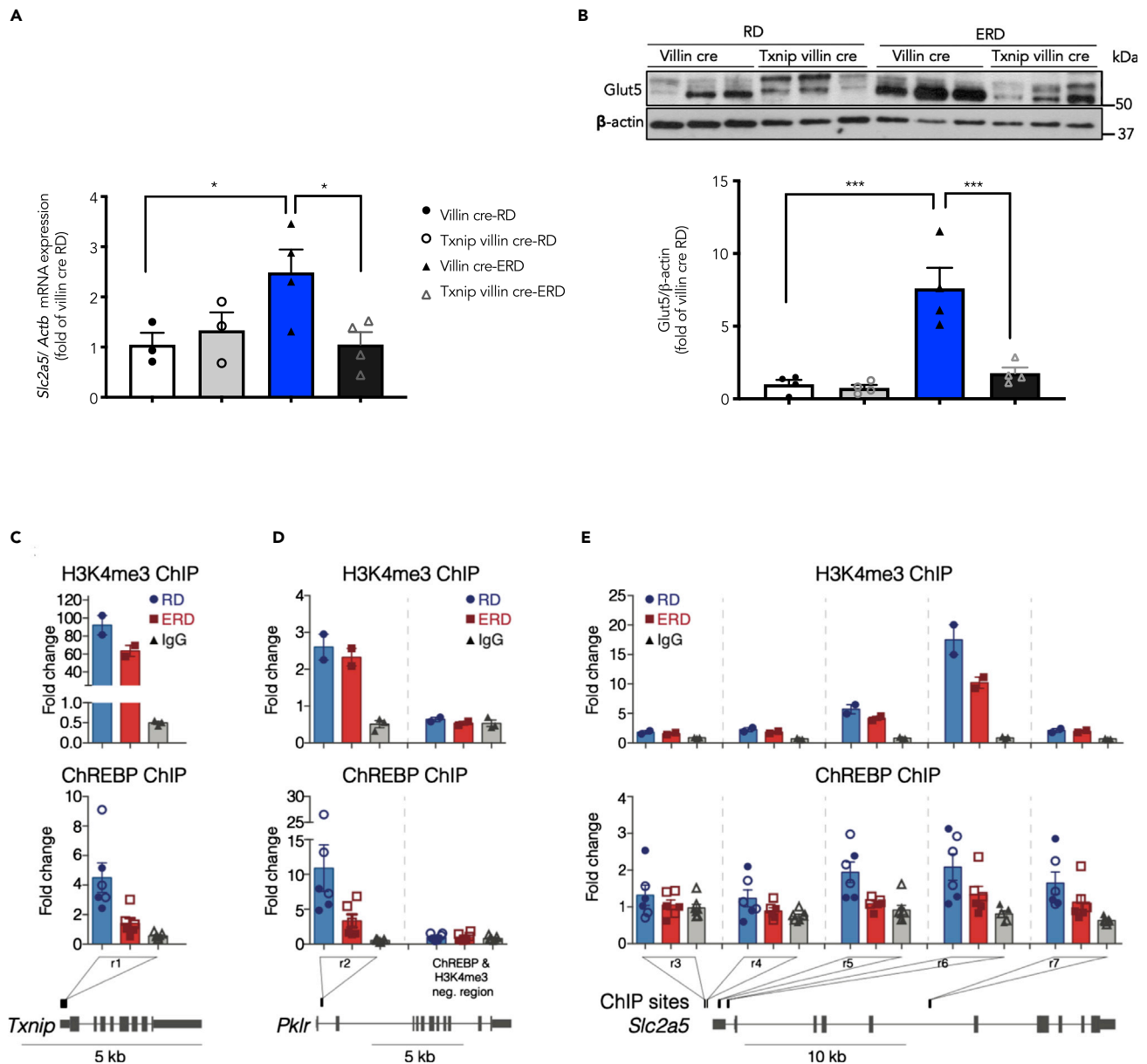


Figure 3. Txnip Is Required for the Energy-Rich Diet-Induced Glut5 Expression

Villin cre and Txnip villin cre mice were placed on RD/ERD for 16 weeks.

(A) Gene expression of *Slc2a5* normalized to *actb* in mucosal lysates extracted from jejunum ($n = 3-4$ /group).

(B) A representative western blot (top) with quantitation (bottom) from the mucosal lysates obtained from jejunum ($n = 4$ /group) showing the Glut5 protein levels. Values are shown as mean \pm SEM. * $p < 0.05$ or *** $p < 0.001$ as calculated by unpaired t test.

(C and D) ChIP for ChREBP and H3K4me3 on intestinal tissues from mice on an RD or an ERD, followed by quantitative PCR to assay enrichment at *Txnip*, *Pklr*, and *Slc2a5* genomic loci. H3K4me3 enrichment shown in the top panel (one of two independent biological replicates shown). Error bars represent the mean \pm SEM of $n = 2$ ChIPs for mice on RD and ERD and $n = 3$ IgG ChIPs. Positive control regions for ChREBP at the (C) *Txnip* promoter (r1) (Poungvarin et al., 2015) and (D) pyruvate kinase L/R (*Pklr*) promoter (r2) (Kim et al., 2017) along with a previously reported ChREBP negative control region (Kim et al., 2017). (E) *Slc2a5* promoter and gene body showing five different ChIP regions assayed (assay was conducted on 2 biological replicates and 3 technical replicates). Regions (r3, r4, and r7) contain previously identified ChREBP-binding sites (Kim et al., 2017; Oh et al., 2018). Regions (r5 and r6) overlap with the *Slc2a5* promoter and are in proximity to previously reported ChREBP-binding sites (Oh et al., 2018). Error bars indicate the mean \pm SEM of two independent ChREBP ChIP experiments for chromatin from $n = 2$ mice on RD ($n = 3$ ChIPs per biological replicate indicated by open or solid circles), $n = 2$ mice on ERD ($n = 3$ ChIPs per biological replicate indicated by open or solid squares), and control IgG ($n = 3$ to 4 ChIPs per biological replicate indicated by open or solid gray triangles) with either RD or ERD chromatin. Two of seven IgG samples for r4 have undetermined Ct values and therefore are not shown. Genomic loci shown are from University of Santa Cruz Genome Browser (UCSC), mm10.

See also Figures S3 and S4.

enrichment of chromatin marks such as H3K4me1 and H3K27ac, which are consistent with a potential role as an enhancer element (Creyghton et al., 2010). We then assayed ChREBP enrichment at the *Slc2a5* promoter and gene body at previously reported ChREBP-binding regions (r3, r4, r7) (Kim et al., 2017; Oh et al., 2018). We noticed ChREBP enrichment at three of five regions in mice fed an RD (r5, r6, and r7) and in two of five regions in mice fed an ERD (r6 and r7) (Figure 3E, bottom panel). We then determined if there was a difference in ChREBP enrichment in mice fed an RD compared with an ERD. In one of five regions examined (r5), we observed a reduced trend in ChREBP-bound chromatin in mice fed an ERD compared with an RD (Figure 3E, bottom panel). It is also notable that in our ChREBP control regions (*Txnip* and *Pklr* promoters) we also observed a decreased trend in ChREBP-bound chromatin in mice fed an ERD compared with an RD (Figures 3C and 3D, bottom panel). ChREBP has been described to have a role as a transcriptional activator or repressor on gene expression (Adamson et al., 2006; Bricambert et al., 2010; Caron et al., 2013; Jeong et al., 2011; Noordeen et al., 2010; Sae-Lee et al., 2016). Thus, the decrease in ChREBP binding at the *Txnip* and *Slc2a5* promoters in mice fed an ERD suggests that the ERD-induced increase of *Txnip* (Figure 1H) and *Slc2a5* (Figure 3A) expression likely functions by an alternative transcriptional mechanism that has yet to be identified. Furthermore, we did not study if loss or gain in *Txnip* regulates methylation of the *Slc2a5* gene. Future comprehensive studies of promoter and enhancer regulation could support the role of changes in *Txnip* level in gene regulation.

Txnip Interacts Endogenously with Rab11a and Is Needed for Apical Localization of Glut5

In addition to augmenting *Glut5* gene and protein expressions, we also studied another potential mechanism for how *Txnip* might promote fructose uptake under ERD. Rab11a, a GTPase Rab-family member that plays a role in membrane trafficking and vesicle formation, is crucial for the apical localization of *Glut5* in the intestinal epithelial cells (Patel et al., 2015). An interaction between *Txnip* and Rab11a was suggested in mass spectrometry data from an unbiased proteomics experiment in our previous studies (Lee et al., 2014). As Rab11a-mediated *Glut5* trafficking to the apical membrane is necessary for fructose uptake (Patel et al., 2015), we speculated that *Txnip* could be facilitating the apical localization of *Glut5* by forming a super-complex with Rab11a. To assess the difference in the co-localization of these proteins in the jejunum of RD and ERD mice, we performed an imaging analysis with dSTORM, a super-resolution digital microscope. A major advantage of using STORM is that it combines high-accuracy localization of the individual fluorophores in three dimensions, allowing for the most precise visualization of molecular interactions at the nanoscopic level (Schmider et al., 2019). We compared the effects of an RD and ERD on the colocalization of *Txnip* with *Glut5* (Figure 4A) or Rab11a at the apical brush border (Figure 4B). The apical brush border was selected using the dSTORM acquisitions where we selected the region of interest (ROI) from the apical side of the tissue to the nuclei. Clus-DoC was then used to determine the colocalization of *Txnip* with either *Glut5* (Figure 4A) or Rab11a (Figure 4B). Localization maps and colocalization maps of *Txnip* relative to *Glut5* or Rab11a from ERD- or RD-fed mice are shown (left panels). Frequency histograms from all tissue sections analyzed are shown (middle graphs). The colocalization of *Txnip* with *Glut5* was increased over 3-fold in ERD-fed mice compared with RD-fed mice (right panels, Figures 4A and 4B, $p < 0.05$). Although there was colocalization, no significant difference in percentage of colocalization was observed with *Txnip* and Rab11a (Figure 4B). Cluster maps of *Txnip* with *Glut5* or Rab11a for the whole ROIs analyzed are shown in Figure S5, along with the analysis of various cluster properties of *Glut5* and *Txnip* clusters that did not change. These results suggest that ERD may increase fructose transport by increasing the number of *Txnip*/*Glut5* interactions in the apical brush border.

We also performed confocal microscopy with Airyscan mode (for super-resolution images) on the cryostat sections obtained from *Txnip* WT and KO mice that were fed RD/ERD for 1 month to assess the localization of *Glut5* in enterocytes. As shown in Figure 4C, we saw that the intensity of *Glut5* staining was elevated at the apical brush border of WT-ERD versus WT-RD (for quantified cellular *Glut5* expression, please refer to Figures 3B and 4A). Notably, *Glut5* appeared to be located in vesicles in the *Txnip* KO enterocytes, suggesting that *Txnip* is required for *Glut5* apical localization.

Conclusion

These data collectively demonstrate that a chronic high-energy diet promotes acute fructose absorption from the intestine and the arrestin domain protein *Txnip* in intestinal epithelial cells plays a crucial role in this process. As seen in Figure 5, we show two molecular mechanisms for this, which we speculate may be working in concert. First, a high-energy diet increases *Glut5* protein and gene expression, and *Txnip* is required for this process. Second, by forming a complex with Rab11a as well as *Glut5*, *Txnip*

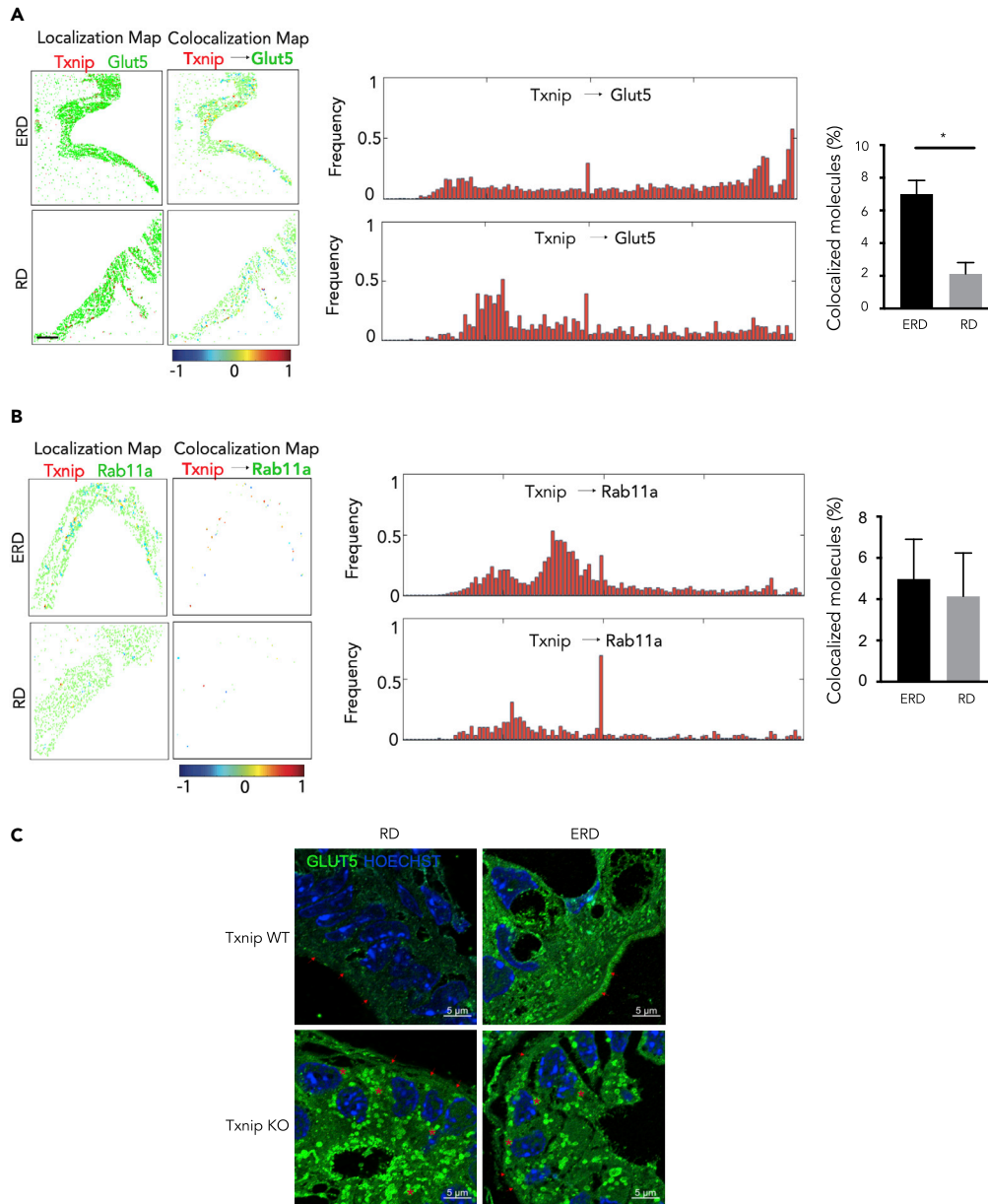


Figure 4. Txnip Interacts with Rab11a and Is Needed for Apical Localization of Glut5

Semi-thin sections (1 μ M) from the small intestine of mice were imaged following ERD or RD using two-color dSTORM. Localization data was analyzed using the Clus-DoC algorithm. Representative images of Txnip and Glut5 and Txnip and Rab11a are shown.

(A) Localization maps for Txnip (red) and Glut5 (green) and colocalization maps for Txnip relative to Glut5 (right panels). Txnip molecules are color-coded according to their degree of colocalization (DoC) scores (color scale bar at bottom). Frequency histograms of DoC scores of all molecules for Txnip from all cells analyzed (middle panels). The percent colocalization of Txnip molecules with Glut5 is shown in the bar graph.

(B) Localization maps, histograms, and bar graphs for the colocalization of Txnip (red) and Rab11a (green). Statistical significance was assessed by two-way ANOVA with multiple comparisons and a Tukey post-test with significance indicated by * $p < 0.05$. Bars show mean \pm SEM from 5–13 ROIs over 3 separate mice (scale bar, 10 μ m). See Figure S5 for more details.

(C). Representative images showing the distribution of Glut5 in enterocytes of Txnip WT and KO mice. One-micron sections from jejunum of RD- or ERD-fed Txnip WT and KO mice ($n = 3$ mice/group) were stained for Glut5. Expression of Glut5 (green) is remarkably elevated at the apical brush border (red arrows) of WT-ERD versus WT-RD. Notably, Glut5 is trapped in vesicles (as shown by *) in the Txnip KO enterocytes. Scale bars, 5 μ m, magnification = 63 \times with Airyscan.

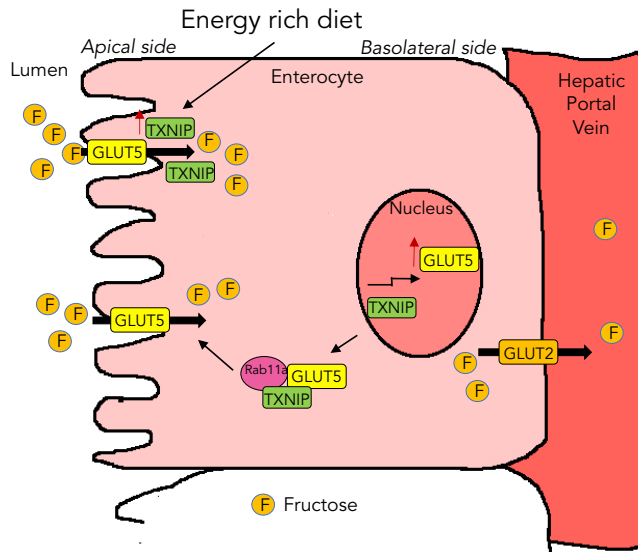


Figure 5. Schematic Representation of Intestinal Fructose Absorption

Energy-rich diet increases intestinal Txnip expression, which in turn increases fructose absorption by elevating both Glut5 protein and gene expressions. Second, Txnip binds with Rab11a, a small GTPase protein essential for Glut5 apical localization, to potentially promote Glut5 trafficking to the apical surface for more fructose uptake.

may be promoting Glut5 trafficking to the apical membrane for enhanced fructose uptake. Thus, our findings suggest that an ERD increases absorption of fructose. This could then have synergistic effects in the liver by promoting more hepatic *de novo lipogenesis*, a key factor in the pathogenesis of metabolic diseases (Schwarz et al., 2017). It is important to note that although the basal level of Txnip is sufficient to conduct fructose absorption and that the higher expression of Txnip leads to increased fructose absorption, this does not prove that the increase in Txnip was solely responsible for the increased fructose absorption. Our study cannot exclude other possibilities that could have been driven by ERD.

Limitations of the Study

The experiments in this study did not isolate high fat content from the moderate sucrose content of the ERD. Chronic fructose consumption can increase acute fructose absorption (Dotimas et al., 2016), and thus the modest amount of fructose in the ERD may be partially responsible for inducing the acute fructose absorption effect. However, our experiments show that, in this model of metabolic disease, Txnip is a molecular mediator of an increase in acute fructose absorption. Future experiments will attempt to isolate an HFD away from all dietary fructose, to determine if high fat alone can promote fructose absorption.

Resource Availability

Lead Contact

Correspondence and requests for materials should be addressed to the Lead Contact, Richard T. Lee (Richard_lee@harvard.edu).

Materials Availability

No new unique reagents were generated in this study. The mice for conditional deletion of Txnip were previously generated by our laboratory and deposited for the public at jax.org.

Data and Code Availability

No dataset or codes were used in this study. The primer sequences used for the ChIP assays were obtained from various literature, and they are listed as well as cited in the Transparent Methods.

METHODS

All methods can be found in the accompanying [Transparent Methods supplemental file](#).

SUPPLEMENTAL INFORMATION

Supplemental Information can be found online at <https://doi.org/10.1016/j.isci.2020.101521>.

ACKNOWLEDGMENTS

Supported by NIH/NIDDK to R.T.L. (1R01DK107396) and J.K.K. (5U2C-DK093000), the Glenn Foundation for Medical Research to A.J.W., and Diabetes Canada Post-Doctoral Fellowship to A.S. (PF-3-16-5176-AS). R.J.S. was supported by National Institutes of Health—1R01AR065538, 1R01CA193520, R01DK062472, and S10RR027931 and the MGH Molecular Imaging Core. A.B.S. was supported by National Institutes of Health—K01DK089145 and R01DK062472. We would also like to thank the Harvard Center for Biological Imaging (CBI) core for their technical advice and guidance with image processing.

AUTHOR CONTRIBUTIONS

Conceptualization, R.T.L. and A.S.; Methodology, A.S., S.D., J.K.K., A.J.W., R.J.S., and R.T.L.; Supervision: A.S., S.D., J.K.K., A.J.W., R.J.S., and R.T.L.; Investigation, A.S., S.D., E.M.R., J.P.L., A.B.S., N.N., H.H., C.V., R.H.F., and H.N.; Formal Analysis, A.S., S.D., A.B.S., J.P.L., N.N., C.V. R.H.F., and H.N.; Writing – Original Draft, A.S. and R.T.L.; Writing – Review and Editing, A.S., S.D., A.B.S., J.P.L., N.N., E.M.R., H.H., C.V., J.K.K., A.J.W., R.J.S., and R.T.L.

DECLARATION OF INTERESTS

The authors declare no competing interests.

Received: March 30, 2020

Revised: July 16, 2020

Accepted: August 28, 2020

Published: September 25, 2020

REFERENCES

- Adamson, A.W., Suchankova, G., Rufo, C., Nakamura, M.T., Teran-Garcia, M., Clarke, S.D., and Gettys, T.W. (2006). Hepatocyte nuclear factor-4 α contributes to carbohydrate-induced transcriptional activation of hepatic fatty acid synthase. *Biochem. J.* 399, 285–295.
- Beyaz, S., Mana, M.D., Roper, J., Kedrin, D., Saadatpour, A., Hong, S.J., Bauer-Rowe, K.E., Xifaras, M.E., Akkad, A., Arias, E., et al. (2016). High-fat diet enhances stemness and tumorigenicity of intestinal progenitors. *Nature* 531, 53–58.
- Bray, G.A., Nielsen, S.J., and Popkin, B.M. (2004). Consumption of high-fructose corn syrup in beverages may play a role in the epidemic of obesity. *Am. J. Clin. Nutr.* 79, 537–543.
- Bricambert, J., Miranda, J., Benhamed, F., Girard, J., Postic, C., and Dentin, R. (2010). Salt-inducible kinase 2 links transcriptional coactivator p300 phosphorylation to the prevention of ChREBP-dependent hepatic steatosis in mice. *J. Clin. Invest.* 120, 4316–4331.
- Caron, S., Huaman Samanez, C., Dehondt, H., Ploton, M., Briand, O., Lien, F., Dorchies, E., Dumont, J., Postic, C., Cariou, B., et al. (2013). Farnesoid X receptor inhibits the transcriptional activity of carbohydrate response element binding protein in human hepatocytes. *Mol. Cell Biol.* 33, 2202–2211.
- Chatterjee, S., Khunti, K., and Davies, M.J. (2017). Type 2 diabetes. *Lancet* 389, 2239–2251.
- Chen, J., Jing, G., Xu, G., and Shalev, A. (2014). Thioredoxin-interacting protein stimulates its own expression via a positive feedback loop. *Mol. Endocrinol.* 28, 674–680.
- Chutkow, W.A., Patwari, P., Yoshioka, J., and Lee, R.T. (2008). Thioredoxin-interacting protein (Txnip) is a critical regulator of hepatic glucose production. *J. Biol. Chem.* 283, 2397–2406.
- Creyghton, M.P., Cheng, A.W., Welstead, G.G., Kooistra, T., Carey, B.W., Steine, E.J., Hanna, J., Lodato, M.A., Frampton, G.M., Sharp, P.A., et al. (2010). Histone H3K27ac separates active from poised enhancers and predicts developmental state. *Proc. Natl. Acad. Sci. U S A* 107, 21931–21936.
- Dotimas, J.R., Lee, A.W., Schmider, A.B., Carroll, S.H., Shah, A., Bilen, J., Elliott, K.R., Myers, R.B., Soberman, R.J., Yoshioka, J., et al. (2016). Diabetes regulates fructose absorption through thioredoxin-interacting protein. *Elife* 5, e18313.
- Jang, C., Hui, S., Lu, W., Cowan, A.J., Morscher, R.J., Lee, G., Liu, W., Tesz, G.J., Birnbaum, M.J., and Rabinowitz, J.D. (2018). The small intestine converts dietary fructose into glucose and organic acids. *Cell Metab.* 27, 351–361 e353.
- Jeong, Y.S., Kim, D., Lee, Y.S., Kim, H.J., Han, J.Y., Im, S.S., Chong, H.K., Kwon, J.K., Cho, Y.H., Kim, W.K., et al. (2011). Integrated expression profiling and genome-wide analysis of ChREBP targets reveals the dual role for ChREBP in glucose-regulated gene expression. *PLoS One* 6, e22544.
- Khan, T.A., and Sievenpiper, J.L. (2016). Controversies about sugars: results from systematic reviews and meta-analyses on obesity, cardiometabolic disease and diabetes. *Eur. J. Nutr.* 55, 25–43.
- Kim, M., Astapova, I.I., Flier, S.N., Hannou, S.A., Doridot, L., Sargsyan, A., Kou, H.H., Fowler, A.J., Liang, G., and Herman, M.A. (2017). Intestinal, but not hepatic, ChREBP is required for fructose tolerance. *JCI Insight* 2, e96703.
- Lee, S., Min Kim, S., Dotimas, J., Li, L., Feener, E.P., Baldus, S., Myers, R.B., Chutkow, W.A., Patwari, P., Yoshioka, J., et al. (2014). Thioredoxin-interacting protein regulates protein disulfide isomerases and endoplasmic reticulum stress. *EMBO Mol. Med.* 6, 732–743.
- Lyssiotis, C.A., and Cantley, L.C. (2013). Metabolic syndrome: F stands for fructose and fat. *Nature* 502, 181–182.
- Malik, V.S., Popkin, B.M., Bray, G.A., Despres, J.P., Willett, W.C., and Hu, F.B. (2010). Sugar-sweetened beverages and risk of metabolic syndrome and type 2 diabetes: a meta-analysis. *Diabetes Care* 33, 2477–2483.
- Noordeen, N.A., Khera, T.K., Sun, G., Longbottom, E.R., Pullen, T.J., da Silva Xavier, G., Rutter, G.A., and Leclerc, I. (2010). Carbohydrate-responsive element-binding protein (ChREBP) is a negative regulator of ARNT/HIF-1 β gene expression in pancreatic islet beta-cells. *Diabetes* 59, 153–160.

- Oh, A.R., Sohn, S., Lee, J., Park, J.M., Nam, K.T., Hahm, K.B., Kim, Y.B., Lee, H.J., and Cha, J.Y. (2018). ChREBP deficiency leads to diarrhea-predominant irritable bowel syndrome. *Metabolism* **85**, 286–297.
- Parikh, H., Carlsson, E., Chutkow, W.A., Johansson, L.E., Storgaard, H., Poulsen, P., Saxena, R., Ladd, C., Schulze, P.C., Mazzini, M.J., et al. (2007). TXNIP regulates peripheral glucose metabolism in humans. *PLoS Med.* **4**, e158.
- Patel, C., Douard, V., Yu, S., Gao, N., and Ferraris, R.P. (2015). Transport, metabolism, and endosomal trafficking-dependent regulation of intestinal fructose absorption. *FASEB J.* **29**, 4046–4058.
- Patwari, P., and Lee, R.T. (2012). An expanded family of arrestins regulate metabolism. *Trends Endocrinol. Metab.* **23**, 216–222.
- Poungvarin, N., Chang, B., Imamura, M., Chen, J., Moolsuwan, K., Sae-Lee, C., Li, W., and Chan, L. (2015). Genome-Wide analysis of ChREBP binding sites on male mouse liver and white adipose chromatin. *Endocrinology* **156**, 1982–1994.
- Sae-Lee, C., Moolsuwan, K., Chan, L., and Poungvarin, N. (2016). ChREBP regulates itself and metabolic genes implicated in lipid accumulation in beta-cell line. *PLoS One* **11**, e0147411.
- Schmider, A.B., Vaught, M., Bauer, N.C., Elliott, H.L., Godin, M.D., Ellis, G.E., Nigrovic, P.A., and Soberman, R.J. (2019). The organization of leukotriene biosynthesis on the nuclear envelope revealed by single molecule localization microscopy and computational analyses. *PLoS One* **14**, e0211943.
- Schwarz, J.M., Clearfield, M., and Mulligan, K. (2017). Conversion of sugar to fat: is hepatic de Novo lipogenesis leading to metabolic syndrome and associated chronic diseases? *J. Am. Osteopath. Assoc.* **117**, 520–527.
- Shao, W., Yu, Z., Chiang, Y., Yang, Y., Chai, T., Foltz, W., Lu, H., Fantus, I.G., and Jin, T. (2012). Curcumin prevents high fat diet induced insulin resistance and obesity via attenuating lipogenesis in liver and inflammatory pathway in adipocytes. *PLoS One* **7**, e28784.
- Soeters, M.R., and Soeters, P.B. (2012). The evolutionary benefit of insulin resistance. *Clin. Nutr.* **31**, 1002–1007.
- Softic, S., Gupta, M.K., Wang, G.X., Fujisaka, S., O'Neill, B.T., Rao, T.N., Willoughby, J., Harbison, C., Fitzgerald, K., Ilkayeva, O., et al. (2017). Divergent effects of glucose and fructose on hepatic lipogenesis and insulin signaling. *J. Clin. Invest.* **127**, 4059–4074.
- Spindel, O.N., World, C., and Berk, B. (2011). Thioredoxin Interacting Protein (TXNIP): redox dependent and independent regulatory mechanisms. *Antioxid. Redox Signal.* **16**, 587–596.
- Sverdlov, A.L., Chan, W.P., Procter, N.E., Chirkov, Y.Y., Ngo, D.T., and Horowitz, J.D. (2013). Reciprocal regulation of NO signaling and TXNIP expression in humans: impact of aging and ramipril therapy. *Int. J. Cardiol.* **168**, 4624–4630.
- Tappy, L., and Le, K.A. (2010). Metabolic effects of fructose and the worldwide increase in obesity. *Physiol. Rev.* **90**, 23–46.
- Waldhart, A.N., Dykstra, H., Peck, A.S., Boguslawski, E.A., Madaj, Z.B., Wen, J., Veldkamp, K., Hollowell, M., Zheng, B., Cantley, L.C., et al. (2017). Phosphorylation of TXNIP by AKT mediates acute influx of glucose in response to insulin. *Cell Rep.* **19**, 2005–2013.
- Wu, N., Zheng, B., Shaywitz, A., Dagon, Y., Tower, C., Bellinger, G., Shen, C.H., Wen, J., Asara, J., McGraw, T.E., et al. (2013). AMPK-dependent degradation of TXNIP upon energy stress leads to enhanced glucose uptake via GLUT1. *Mol. Cell* **49**, 1167–1175.
- Zietek, T., Rath, E., Haller, D., and Daniel, H. (2015). Intestinal organoids for assessing nutrient transport, sensing and incretin secretion. *Sci. Rep.* **5**, 16831.

Supplemental Information

Thioredoxin Interacting Protein Is Required for a Chronic Energy-Rich Diet to Promote Intestinal Fructose Absorption

Anu Shah, Sezin Dagdeviren, Jordan P. Lewandowski, Angela B. Schmider, Elisabeth M. Ricci-Blair, Niranjana Natarajan, Henna Hundal, Hye Lim Noh, Randall H. Friedline, Charles Vidoudez, Jason K. Kim, Amy J. Wagers, Roy J. Soberman, and Richard T. Lee

FIGURE S1: ERD increases acute fructose absorption in the presence of glucose or mannitol in the administering solution and ERD also raises ^{13}C -F1P levels. Related to Fig 1.

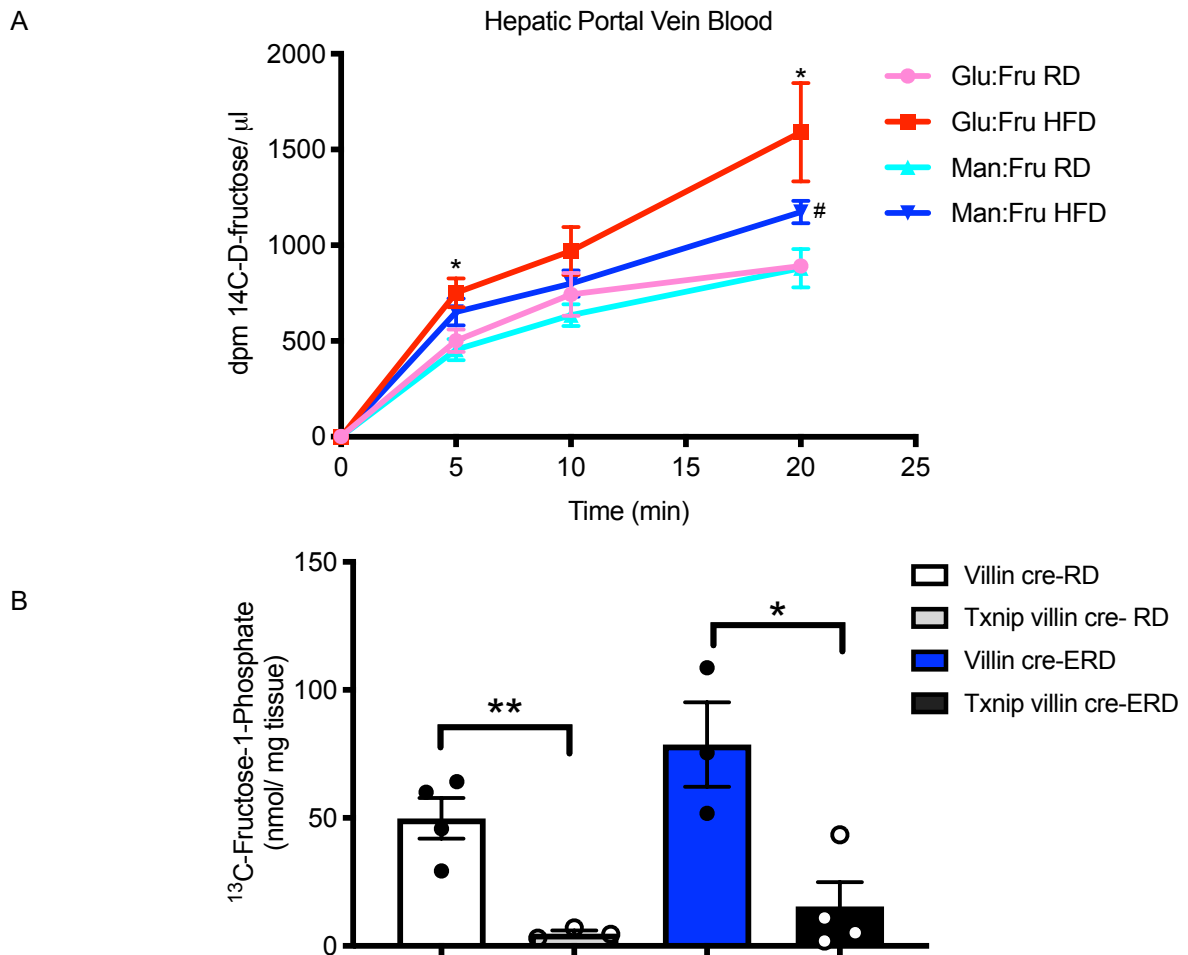


Figure S1. ERD increases acute fructose absorption in the presence of glucose or mannitol in the administering solution and ERD also raises ^{13}C -F1P levels. (A) C57BL/6J mice placed on RD or ERD for 8 weeks were subjected to a bolus oral gavage of radiolabeled fructose prepared in cold 1:1 mannitol: fructose (Man:Fru) or 1:1 glucose: fructose (Glu:Fru). Hepatic portal vein blood was obtained 0, 5, 10 or 20 min post gavage. Administration of radioactive fructose prepared in glucose solution elevated fructose absorption (i.e. ^{14}C -fructose+ metabolites) significantly in the ERD-fed mice ($*p < 0.05$ vs Glu:Fru RD) as early as 5 min post- gavage, unlike the mannitol administered group. However, at 20 min, fructose absorption increased significantly in the ERD groups regardless of glucose or mannitol mixed in the administering solution. ($*p < 0.05$ vs Glu:Fru RD, # $p < 0.05$ vs Man:Fru RD, $n = 6$ (5 for time 0 min) /group for each time point). All values are mean \pm SEM and the statistical analyses were performed using an unpaired two-tailed t -test. (B) Txnip villin cre and villin cre mice placed on RD/ ERD for 16 weeks were given bolus intragastric gavage of ^{13}C -fructose to assess ^{13}C -F1P level in the jejunum after 20 min post gavage. All values are mean \pm SEM and the statistical analyses were performed using an unpaired two-tailed t -test where $*p < 0.05$ vs and $**p < 0.01$ ($n = 3-4$ mice/ group).

FIGURE S2: Acute fructose absorption increases with chronic exposure to fructose in the diet. Related to Fig 1.

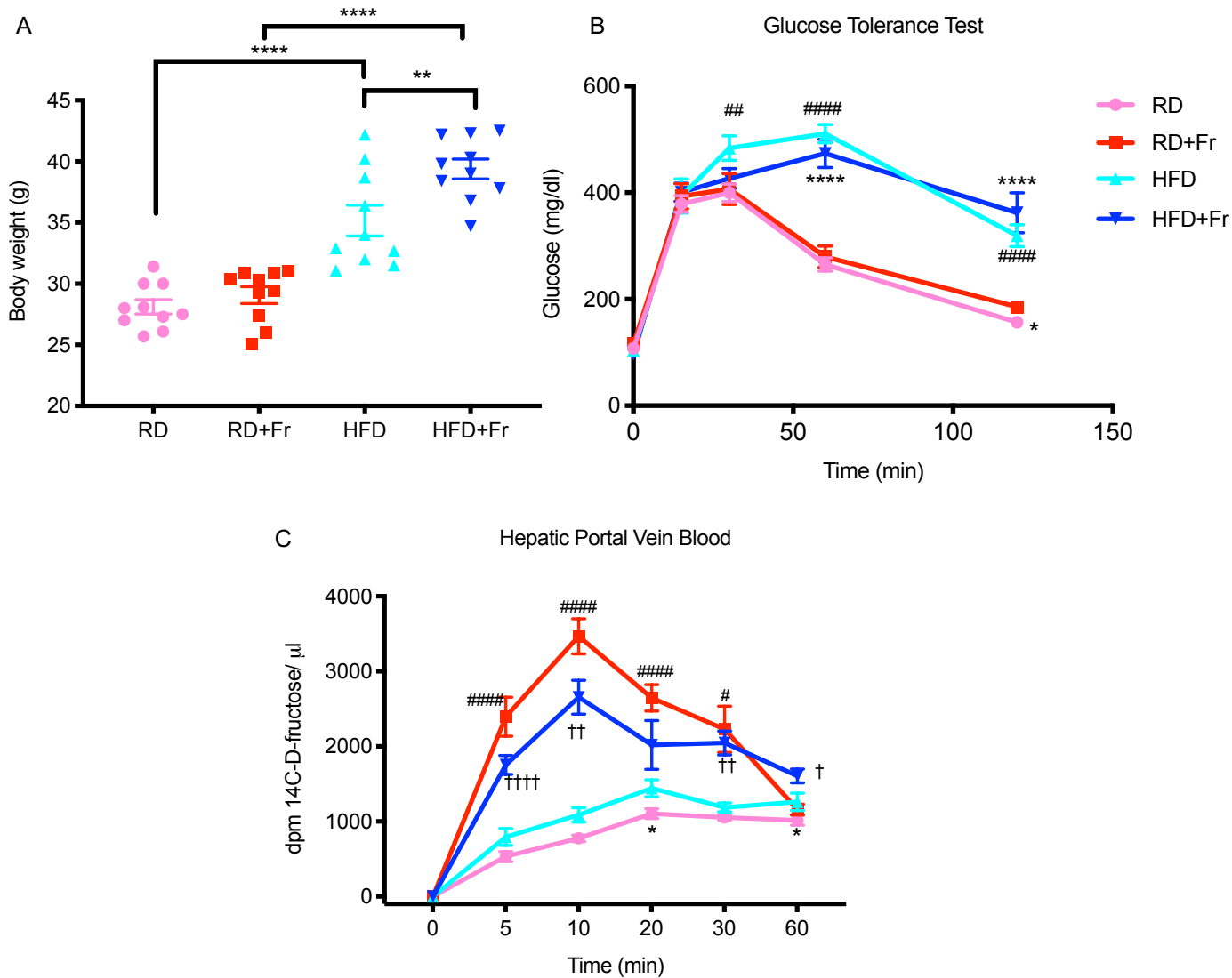


Figure S2. Acute fructose absorption increases with chronic exposure to fructose in the diet. A 4-week long study on RD or ERD-fed mice in the presence or absence of 30% fructose in water caused (A) a significant increase in body weight in mice fed a ERD as compared to ERD-fed mice with *ad libitum* access to water only (n=10 mice/ group, **p<0.01, ****p<0.0001). (B) Glucose tolerance tests illustrate that fructose in drinking water did not worsen glucose intolerance by ERD in 4 weeks (n=10 mice/ group, *p<0.05, ****p<0.0001 vs RD+Fr, ##p<0.01 and #####p<0.0001 vs RD). (C) Kinetics of fructose (i.e. 14C-fructose+ metabolites) absorption in hepatic portal vein blood assessed at 0, 5, 10, 20, 30, and 60 min post-oral gavage of radiolabeled fructose. For each time point, n=6 mice/ group were sacrificed to harvest tissues for analysis. Consistent with our previous study (Dotimas et al., 2016), fructose absorption peaked at 20-min after radiolabeled fructose gavage in mice that did not receive fructose in drinking water. However, mice that received fructose in drinking water had a peak portal vein absorption at 10 minutes, in the presence or absence of ERD. All values are mean± SEM, and the statistical analysis was performed using an unpaired two-tailed *t*-test; n=6 for each group at each time-point, #p<0.05 and #####p<0.0001 vs RD; †p<0.05, ††p<0.01, ††† p<0.0001 vs ERD.

FIGURE S3: Intestinal Txnip does not alter tissue responsiveness to nitric oxide. Related to Fig 3.

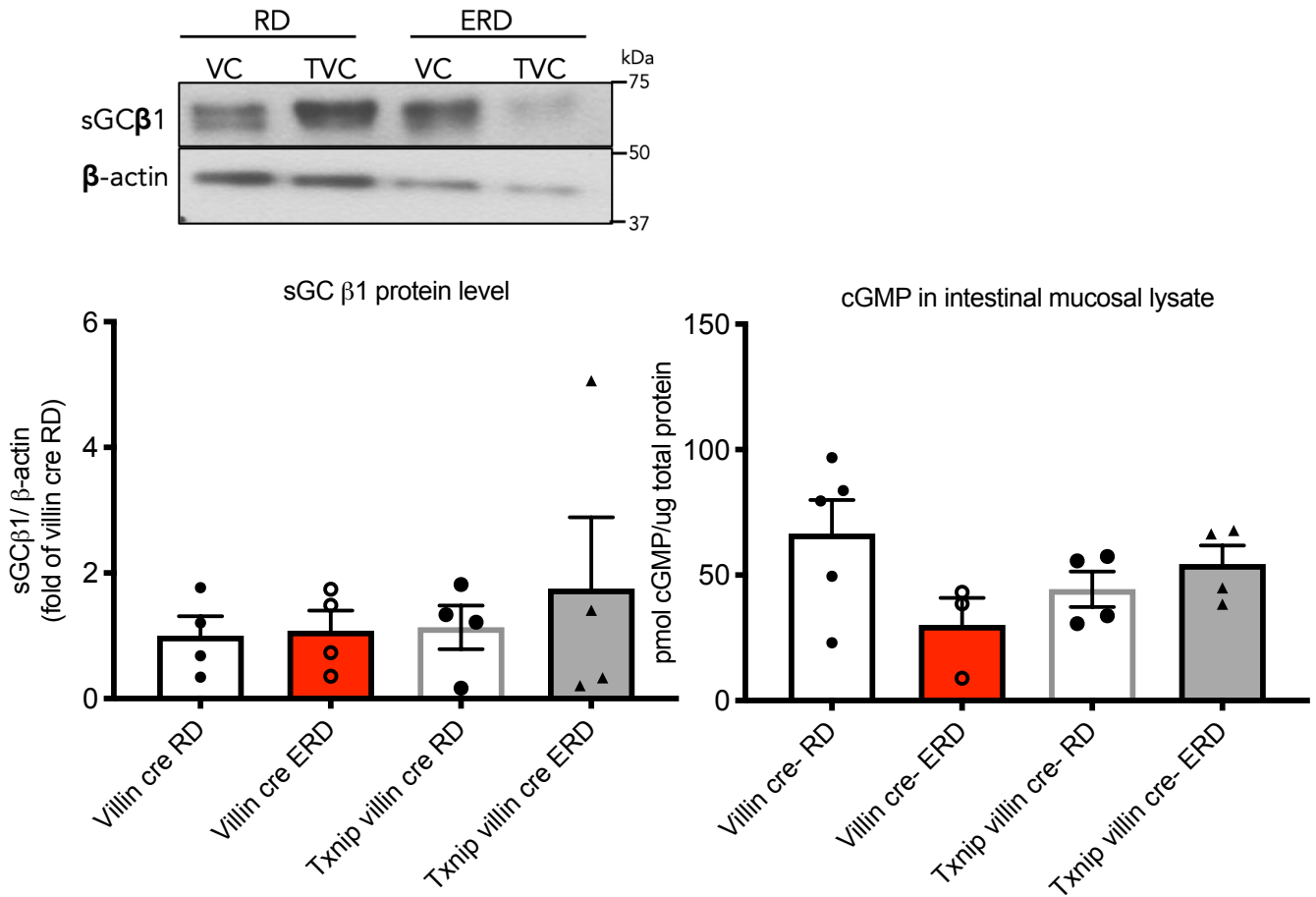


Figure S3. Intestinal Txnip does not alter tissue responsiveness to nitric oxide. Intestinal mucosal lysates from villin cre and Txnip villin cre mice placed on a RD were not significantly different in soluble guanylate cyclase β1(sGCβ1) protein expression (left panel, n=4) or its the activation (via cGMP activity) (right panel, n=3-5) after ERD feeding. Moreover, intestinal Txnip expression did not affect these parameters. All the values are mean± SEM and the statistical analyses were performed using an unpaired two-tailed *t*-test, with no significant differences found.

FIGURE S4: Chromatin immunoprecipitation (ChIP) on intestinal tissue from mice with H2O (n=2) and mice with fructose (n=1) for ChREBP, H3K4me3, and IgG followed by quantitative PCR (QPCR) to assay enrichment at three different loci. Related to Fig 3.

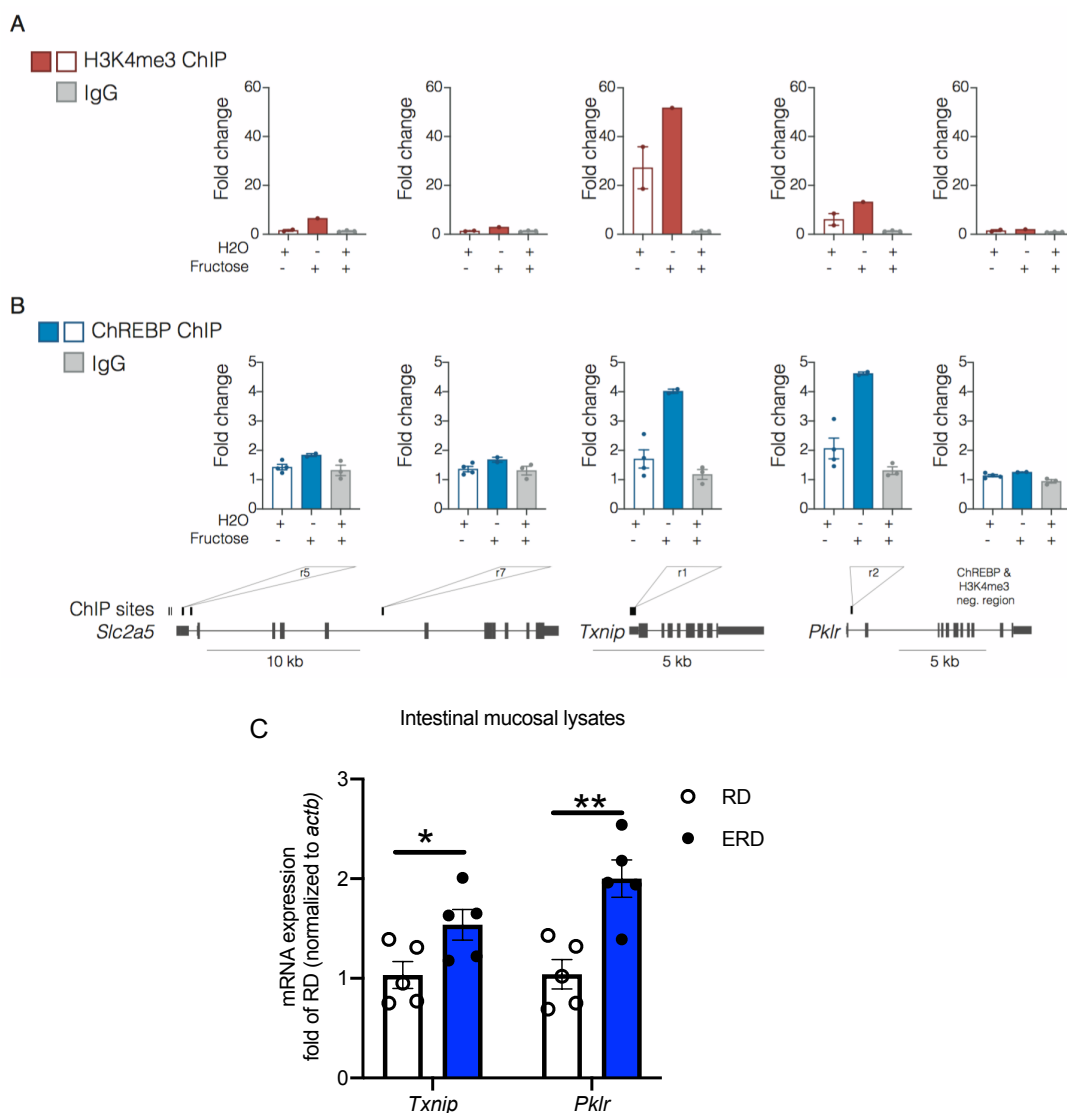


Figure S4. Chromatin immunoprecipitation (ChIP) on intestinal tissue from mice with H2O (n=2) and mice with fructose (n=1) for ChREBP, H3K4me3, and IgG followed by quantitative PCR (QPCR) to assay enrichment at three different loci. (A) H3K4me3 ChIP in H2O treated (n=2 ChIPs), fructose treated (n=1 ChIP), and IgG samples (n=3 ChIPs). Enrichment assayed at *Slc2a5*, *Txnip*, and *Pklr*. (B) ChREBP ChIP in H2O treated (n=4 ChIPs), fructose treated (n=2 ChIPs), and IgG samples (n=3 ChIPs). *Slc2a5* promoter and gene body showing two different ChIP regions assayed r5 and r7, which is previously identified ChREBP binding region (Kim et al., 2017). r5 is in proximity to two previously reported ChREBP binding sites (Oh et al., 2018). Positive control regions for ChREBP at the *Txnip* promoter (r1) (Poungvarin et al., 2015) and Pyruvate kinase L/R (*Pklr*) promoter (r2) (Kim et al., 2017). And a ChREBP negative control region at the *Pklr* promoter (Kim et al., 2017). The mean is shown and the error bars represent the standard error of the mean. Genomic loci shown are from University of Santa Cruz Genome Browser (UCSC), mm10. (C) Relative gene expression of intestinal *Txnip* and *Pklr* after mice were fed a RD or ERD. All values are mean \pm SEM, and the statistical analysis was performed using an unpaired two-tailed *t*-test; n=5, **p*<0.05 and *p*<0.01 vs RD.**

FIGURE S5: Cluster maps for Txnip with Glut5 and Txnip with Rab11a . Related to Fig 4.

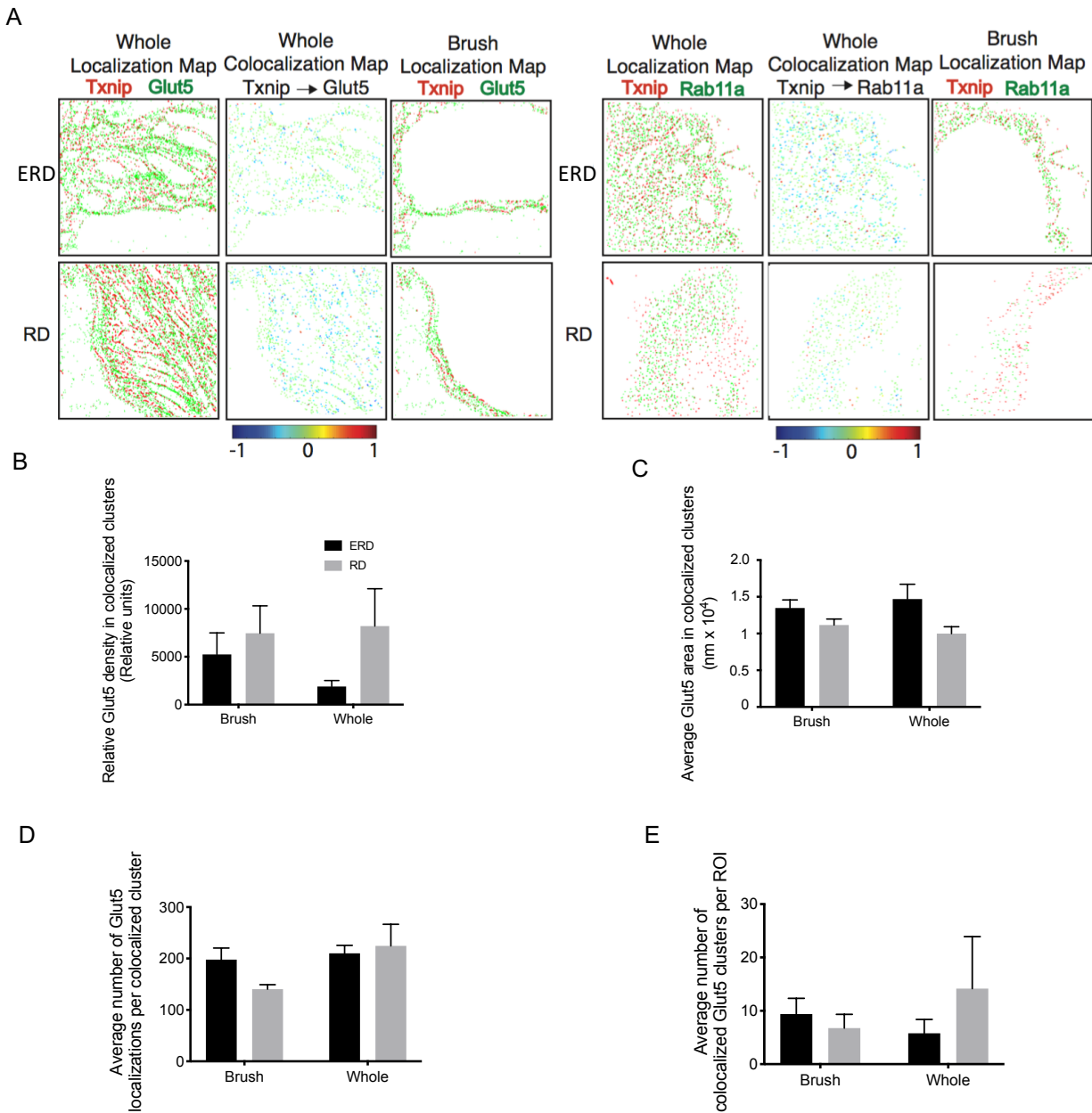


Figure S5. Cluster maps for Txnip with Glut5 and Txnip with Rab11a. (A) Localization maps for Txnip (red) and Glut5 or Rab11 (green) encompassing apical to basolateral brush border (whole) or only apical brush border (brush). Maps for Txnip relative to Glut5 left panels. Txnip localizations are pseudocolor-coded according to their degree of colocalization (DoC) scores (score bar at the bottom). Right panels show localization maps for Txnip and Rab11a. Clusters were defined as having ≥ 10 localizations with a DoC score of ≥ 0.4 for figures B-E. Glut5 cluster properties: (B) relative density; (C) average area; (D) average number of localizations; and (E) average number of cluster per ROI. The relative density of clusters was calculated by dividing the local density within 20 nm of each localization by the average density of the cluster, a measure of the local concentration maxima within the cluster. Statistical significance was assessed by two-way ANOVA with multiple comparisons and a Tukey post-test with significance indicated by $*p < 0.05$. Bars show mean \pm SEM from 5-13 ROIs over 3 separate mice. Scale bar represents 10 μ M.

Table S1. Metabolic profile of RD or ERD-fed mice. Related to Fig 1.

	4-weeks diet		16-weeks diet	
	RD (n=7)	ERD (n=7)	RD (n=14-16)	ERD (n=14-16)
Body weight (g)	28.9±0.2	35.7±1.5**	31.4±0.5	42.7±1.0***
Fasting blood glucose (mg/dL)	117.3±3.8	108.0±9.3	109.2±10.4	115.1±5.7
AUC- Glucose tolerance test (a.u.)	31707.5±1040.8	51019.3±2116.2***	36596.0±989.6	60884.5±1583.6***

Table S1. Metabolic profile of RD or ERD-fed mice. Results are expressed as mean ± SEM (n=7/ group (4 weeks-diet) and n=14-17/group (16 weeks-diet). P-values were calculated using an unpaired student's *t*-test for body weight and fasting glucose, and one-way ANOVA followed by Bonferroni's *post-hoc* test was employed for the AUC from Glucose tolerance test (GTT). **p<0.05 and ***p<0.0001 vs their own RD diet control.

Table S2. Metabolic profile of Txnip villin cre and Villin cre mice. Related to Fig 2.

4-weeks diet	Villin cre		Txnip villin cre	
	RD (n=5)	ERD (n=5)	RD (n=5)	ERD (n=4)
Body weight (g)	25.8±0.8	33.9±1.9**	27.2±0.1	35.9±1.9*
Fasting blood glucose (mg/dL)	116.0±9.0	132.0±5.5	117.2±6.5	132.5±7.7
AUC- Glucose tolerance test (a.u.)	23794.5±722.4	42777.0±1639.0***	24030.0±766.6	34346.3±1058.3***,***
16-weeks diet	Villin cre		Txnip villin cre	
	RD (n=5)	ERD (n=5)	RD (n=5)	ERD (n=3)
Body weight (g)	28.0±0.9	48.5±1.3***	30.8±1.1	51.2±0.8***
Fasting blood glucose (mg/dL)	104.4±5.9	114.4±7.3	117.4±5.4	122.0±17.0
AUC- Glucose tolerance test (a.u.)	30343.5±939.0	53818.5±2483.6***	23788.5±640.2	55617.5±3188.1***

Table S2. Metabolic profile of Txnip villin cre and Villin cre mice. Results are expressed as mean ± SEM (n=4-5/ group (4 weeks-diet) and n=3-5/ group (16 weeks-diet). P-values were calculated using an unpaired student's *t*-test for body weight and fasting glucose, and one-way ANOVA followed by Bonferroni's *post-hoc* test was employed for the AUC from Glucose tolerance test (GTT). *p<0.05, **p<0.01, and ***p<0.001 vs their own regular diet control; ***p<0.001 vs villin cre ERD.

TRANSPARENT METHODS

Animal care and diets

All experiments were conducted in accordance with the Guidelines for the Use and Care of Laboratory Animals and approved by the Harvard University Institutional Animal Care and Use Committee (protocol number 16-05-271 and 16-05-272). All the mice were housed at controlled temperature (20-21°C) on a 12h light/dark cycle. Txnip knockout (KO) mice were generated in our lab and C57Bl/6J was used as Txnip wildtype (WT) control. For fructose absorption studies, C57Bl/6J male mice, subjected to either 4-weeks or 16-weeks of regular (RD) or energy rich diet (ERD), were obtained from JAX. Txnip villin cre (Txnip^{fl/fl} villin cre^{+/-}) mice were generated by breeding Txnip^{fl/fl} mice (Yoshioka et al., 2007), generated in our lab, with villin cre mice (Vil-Cre 1000, JAX). Age-matching villin cre (Txnip^{+/+} cre^{+/-}) mice were used as controls. 7-9 weeks old mice were randomly subjected to RD (Prolab®IsoPro® RMH 3000, 5P75/ 5P76) or ERD (60% kcal HFD, ResearchDiets Inc., D12492), and provided free access to water. In the experiments where mice were supplemented with fructose solution to their diet, 30% fructose solution in drinking water was used.

The number of mice required for the study was determined by using the sample size calculations from the IACUC at Boston University (<https://www.bu.edu/researchsupport/compliance>), and an alpha of 0.05 and statistical power of 90% were used as parameters to estimate the appropriate sample size. All the experiments were performed as independent biological replications (for example: n=3 means three mice), except for the qPCR and ChIP assays that have both biological and technical replications. Moreover, the inclusion and exclusion of data was verified by the Graphpad Outlier calculator (<https://www.graphpad.com/quickcalcs/Grubbs1.cfm>) where alpha=0.05.

In vivo bio-distribution assay with radiolabeled fructose

Intestinal fructose uptake and bio-distribution was assessed as previously described (Dotimas et al., 2016) but with a slight modification. Briefly, 20 minutes after the intragastric administration of 2 µCi [¹⁴C(U)]-D-fructose (Moravek Inc.) in 200µl 30% of non-radioactive fructose/ mannitol, blood samples were collected from tail and portal veins and tissues were harvested. We used mannitol instead of glucose in the administering solution in order to avoid effects of glucose on fructose uptake as shown in Supplemental Figure S1A. Ba(OH)₂ and ZnSO₄ were used to precipitate proteins in plasma, and the supernatants were counted using Ultima Gold Scintillation fluid (PerkinElmer). Similarly, 100-150mg of tissues were homogenized using 10X volume of water and boiled for 10 min at 100°C. The samples were then centrifuged and 500µl of clear supernatant was added to 5 ml scintillation fluid. Pre-weighed intestinal were dissolved in 1ml soluene (Soluene®-350, PerkinElmer) at 55°C for 4h before adding them to 5 ml scintillation fluid. Radioactivity in tissues was measured in the Beckman Coulter LS 6500 Liquid Scintillation Counter.

Glucose tolerance test

Glucose tolerance test (GTT) was performed after overnight fasting. After obtaining body weight and basal blood glucose reading from a tail clip, mice were administered a bolus glucose (2g/kg body weight) intraperitoneally. Blood glucose values were then obtained at 15, 30, 60, 90, and 120 minutes using a Bayer Contour Blood Glucometer.

Metabolic studies

Metabolic changes were measured at the National Mouse Metabolic Phenotyping Center (MMPC) at the University of Massachusetts Medical School. Briefly, mice were individually placed in metabolic cages (TSE-Systems Inc., Bad Homburg, Germany) for 3 days to non-invasively assess their indirect calorimetry and energy balance parameters, including physical activity, food/ water intake, respiratory exchange ratio, and energy expenditure. Whole body fat and lean fat were non-invasively assessed in awake mice via proton magnetic resonance spectroscopy (¹H-MRS) (Echo Medical Systems, Houston, TX). Liver triglycerides, plasma cholesterol, and HDL/ LDL were assessed by the Analytical Core of UMass MMPC.

Immunoblotting

Villi were extracted from the small intestine using the procedure as previously described (Booth and O'Shea, 2002). Immunoblotting on homogenized jejunal samples and villi were performed as described

previously (Shah et al., 2015). For primary antibodies, anti-Txnip (MBL) and anti-Glut5 (EMD Millipore, 07-1406) were used at 1:1000 dilution, and β -actin (Santa Cruz) at 1:10000.

Quantitative PCR analysis

Frozen tissues were homogenized in TRIZOL reagent (Invitrogen) to extract RNA. cDNA synthesis on 1 μ g RNA was performed using the High Capacity cDNA Reverse Transcription kit (Applied Biosystems). The cDNA was then used for real-time PCR analysis using the Taqman Gene Expression System, where the following mouse-specific primers were used: *Txnip* (Mm00452393_m1), *Slc2a5* (Mm00600311_m1), *Pklr* (Mm00443090_m1), and the housekeeping gene, *Actb* (Mm02619580_g1). Relative gene expression was calculated as mentioned before (Dotimas et al., 2016).

Extraction and fructose uptake in intestinal organoids

Intestinal organoids from Txnip WT and KO mice were extracted and maintained according to the protocol previously described by Zietek et al., 2015. Fructose uptake assay was performed on differentiated organoids (proliferated/ budded organoids), from days 5-7, also following the protocol from the same article.

Histology, N-STORM and co-localization analysis

Cryostat sections of jejunum (1- μ m) were incubated overnight in 1:100 dilution of primary antibodies: anti-Txnip (MBL), anti-Glut5 (EMD Millipore, 07-1406) and anti-RAB11A (US Biological, R0009) in PBS containing 0.2 % skim milk and 1% BSA. Tissues were then incubated for 1h at room temperature with 3 μ g/ml secondary antibodies that were made in house to achieve a near ratio of 1:1, antibody: fluorophore, respectively. After nuclei staining with DAPI (1:1000), tissues were fixed with 4% PFA followed by visualization and analysis via Stochastic Optical Reconstruction Microscopy (N-STORM). Briefly, the imaging buffer containing 100 mM 2-mercaptoethanolamine (MEA) and 1% (v/v) GLOX was used to promote photoswitching and reduce photobleaching. An inverted Nikon Ti2 Eclipse STORM 5.0 system with Perfect Focus focal plane lock was used for image acquisition. This system contains a NSTORM quadband filter, and 405, 488, 561, and 647 nm lasers and was equipped with an HP APO TIRF AC 100x/1.49 NA oil objective and ORCA-Flash4.0 SCI CMOS PLUS camera (Hamamatsu Photonics). 15,000 frames for each dye were collected at 30 ms exposure time in continuous mode. Localizations were identified with NIS Elements 5.0 (Nikon Instruments) and exported as tab-delimited text files.

To produce reporter antibodies for dSTORM, donkey anti-rabbit and donkey anti-mouse affinity purified secondary antibodies (H+L chains) (Jackson Laboratory) were conjugated to Cy3B (GE Healthcare) or AF647 dyes, both with carboxylic acid succinimidyl ester moieties. For the conjugation reactions, 240 μ g of the secondary antibody was reacted with 6 μ g of dye in 56 mM carbonic buffer for 2 hours at room temperature. After the reactions, the antibodies were separated from unconjugated dye by gravity filtration through Sephadex G-25 DNA grade size exclusion columns (GE Healthcare) by visual detection. Antibody and dye concentrations were determined using a NanoDrop spectrometer (Thermo Fisher) to record absorbance at 280 nm and at the dye absorbance peak. Antibody concentration was calculated by subtracting the contribution of each dye to absorbance at 280 nm using correction factors provided by the dye manufacturers (Cy3B: 0.09, AF647: 0.03) and the molar extinction coefficient of the antibody (210,000). The final ratio for the donkey-anti-rabbit: Cy3B was 1:2 with antibody concentration of 151 μ g/ μ L. The final ratio for the donkey-anti-mouse:AF647 was 1:5 with antibody concentration of 200 μ g/ μ L.

Clus-DoC analysis of single molecule localizations

We employed Clus-DoC (Pageon et al., 2016), which quantifies colocalization of individual proteins and molecules (localizations) and cluster properties (Schmider, 2019) to analyze dSTORM localization Clus-DoC allows for the user to define the number and DoC threshold.

In brief, co-localization between two proteins (localizations/molecules) is analyzed at the single-molecule level. This coordinate-based co-localization method uses algorithms that detect and save coordinates of single molecules. The spatial distribution surrounding localizations from both proteins of interest is compared to a single point. The density gradients of both proteins are generated. Next, the two distributions (densities) are compared by calculating a rank correlation coefficient where each molecule is assigned a

degree of co-localization (DoC) score ranging from -1 (segregated) to 0 (non-co-localized) to +1 (perfectly co-localized). Finally, because majority of the DoC scores were >0.4 with a peak at 1 (high co-localization), a threshold of 0.4 was used to distinguish co-localized from non-co-localized localizations.

Fructose Isotope gavage and sample collection

Animals were starved for 5h before administering them with 1:1 mixture of unlabeled mannitol and labeled [^{13}C]-fructose (Cambridge Isotope Labs, CLM-1553-PK), 2g/kg each via intragastric gavage. Mice were euthanized 20 min later and their tissues were harvested and frozen in -70°C until extraction.

Metabolite extraction and LC-MS

Tissues were extracted in guidance of the Harvard Small Molecule Mass Spectrometry facility. Briefly, tissues were homogenized with a homogenizer in HPLC grade cold methanol (4°C) before adding HPLC grade chloroform and LC/MS grade water. After centrifugation, the aqueous phases were isolated, dried using nitrogen evaporator and then submitted to the Mass Spectrometry facility. LC-MS analysis was performed using a Thermo Q- Exactive Plus Hybrid Quadrupole- Orbitrap mass spectrometer, coupled with a Thermo UltiMate 3000 LC and a Millipore zic-PHILIC column.

Immunostaining and Confocal Microscopy

Cryostat sections ($1\text{-}\mu\text{m}$) from jejuna of *Txnip* WT and KO mice fed with either RD or ERD for 1 month were incubated with 1:100 dilution of anti-Glut5 (EMD) overnight in 4°C . Incubation with secondary antibody (1:500, goat anti-rabbit Alexa Fluor 488 from Invitrogen) along with 1:1000 Hoechst 33342 was done for 1h at RT. Confocal imaging to assess expression of Glut5 in the tissues was carried out using Zeiss LSM 880 with Airyscan detector (GaAsP-PMT super-resolution detector) at the Harvard Center for Biological Imaging. The Airyscan detector (Huff, 2015) was used to get a high-resolution image of Glut 5 expression in enterocytes and the brush-border membrane using a 63X oil immersion objective.

Chromatin immunoprecipitation (ChIP)

ChIP experiments were performed using the iDeal ChIP-qPCR kit (Diagenode, C01010180) according to the manufacturer's instructions. We performed two independent ChREBP ChIP experiments. We used C57Bl/6J male mice that were fed a RD ($n=2$) or ERD ($n=2$) for 15 weeks. We then extracted approximately 200 mg of mucosal layer from the jejunum and crosslinked the tissue in 1% methanol-free formaldehyde solution (Thermo Scientific, 28906) for 20 min at room temperature with gentle agitation. The isolated chromatin was sheared with a Bioruptor (Diagenode) using 18 cycles of 30 s 'on' and 30 s 'off'. Fresh chromatin was used for multiple individual ChIP reactions. We added either $2\mu\text{g}$ of ChREBP (Abcam, ab92809), $2\mu\text{g}$ of IgG (Diagenode, K02921003), or $2\mu\text{g}$ of H3K4me3 antibodies (Diagenode, K02921004). 1% of the sheared chromatin was retained for the input control. The occupancy of ChREBP and H3K4me3 at the promoters of *Slc2a5*, *Txnip*, and *Pklr* was assessed by real-time qPCR on a ViiA7 Real-Time PCR System (ABI) using FastStart Universal SYBR Green Master (Rox) (ABI, 4913914001) with the following cycling parameters: 95°C for 10min, followed by 40 cycles of 95°C for 10 seconds and 60°C for 30 seconds. The enrichment values were determined by the $\Delta\Delta\text{Ct}$ method of normalized IP over normalized input using the baseline primer pairs F-baseline and R-baseline (Vokes et al., 2007), where $\Delta\Delta\text{C}(t) = \Delta\text{C}(t)\text{ChIP} - \Delta\text{C}(t)\text{Input}$; $\Delta\text{C}(t)\text{ChIP} = \text{C}(t)\text{experimental primer} - \text{C}(t)\text{baseline primer}$ in the ChIP sample and $\Delta\text{C}(t)\text{Input} = \text{C}(t)\text{experimental primer} - \text{C}(t)\text{baseline primer}$ in the input sample. We used the following primers for qPCR:

F-r1: GGGGTTTCCAGAGTTTCTCC; R-r1: CTCCGTAAGTCAGGGCTTG (Poungvarin et al., 2015)

F-r2: TTTGATCCAGGCTCTGCAGAC; R-r2: TCTTGCCAATGGAAGCCTTG (Kim et al., 2017)

F-r3: GAT TTC CTG CCG CAT TCA GA; R-r3: TTT TCAGAC CTC CCA GAT GGA (Oh et al., 2018)

F-r4: TCC ATC CAC ACA CTTTCA AAC; R-r4: CAA GCC ACG GCC AAC AG (Oh et al., 2018)

F-r5: AGTTGAAGAGCCACCGTGTT; R-r5: AGTGTAGATCCGCTCGGGTA

F-r6: AGCACAGGCAATCCGTA_{CTC}; R-r6: GCCTAGTGTTTCCCACCACA
F-r7: GGGACTGAGAAACATCCGGG; R-r7: TGTTGCCCAAGGTGCTGATA (Kim et al., 2017)

F-neg: TGGACATTTGACTCCAGAGC; R-neg: AACATGGAGAAGAAGGCAGTG (Kim et al., 2017)

F-baseline: CTGGCCTCCATACACACATA; R-baseline: AGTCAGCAGGATCCACACTT (Vokes et al., 2007)

ChREBP ChIP response to a classical stimuli (fructose) was assessed in C57Bl/6J mice following the protocol described by Kim *et al.* (Kim et al., 2017).

Statistical analyses

Data are presented as mean \pm SEM, unless otherwise stated. P-values were calculated using an unpaired student's *t*-test since we were specifically comparing 2 groups at a time (such as comparison between the fructose absorption due to two different diets on the same strain of mice, or difference in the absorption by two different strains of mice placed on same diet). To calculate the statistical significance of AUC for glucose tolerance test (GTT), one-way ANOVA followed by Bonferroni *post hoc* method was used (Graphpad Prism, version 7.0). Two-way ANOVA with multiple comparisons and a Tukey post-test was employed for the colocalization studies via STORM, where significance was indicated by * $p < 0.05$.

SUPPLEMENTAL REFERENCES

Booth, C., and O'Shea, J.A. (2002). Isolation and Culture of Intestinal Epithelial Cells. In Culture of specialized cells, R.I. Freshney, and M.G. Freshney, eds. (New York: Wiley-Liss), pp. xv, 461 p.

Dotimas, J.R., Lee, A.W., Schmider, A.B., Carroll, S.H., Shah, A., Bilen, J., Elliott, K.R., Myers, R.B., Soberman, R.J., Yoshioka, J., *et al.* (2016). Diabetes regulates fructose absorption through thioredoxin-interacting protein. *Elife* 5.

Huff, J. (2015). The Airyscan detector from ZEISS: confocal imaging with improved signal-to-noise ratio and super-resolution. *Nature Methods* 12, i-ii.

Kim, M., Astapova, I., Flier, S.N., Hannou, S.A., Doridot, L., Sargsyan, A., Kou, H.H., Fowler, A.J., Liang, G., and Herman, M.A. (2017). Intestinal, but not hepatic, ChREBP is required for fructose tolerance. *JCI Insight* 2.

Oh, A.R., Sohn, S., Lee, J., Park, J.M., Nam, K.T., Hahm, K.B., Kim, Y.B., Lee, H.J., and Cha, J.Y. (2018). ChREBP deficiency leads to diarrhea-predominant irritable bowel syndrome. *Metabolism* 85, 286-297.

Pageon, S.V., Nicovich, P.R., Mollazade, M., Tabarin, T., and Gaus, K. (2016). Clus-DoC: a combined cluster detection and colocalization analysis for single-molecule localization microscopy data. *Mol Biol Cell* 27, 3627-3636.

Poungvarin, N., Chang, B., Imamura, M., Chen, J., Moolsuwan, K., Sae-Lee, C., Li, W., and Chan, L. (2015). Genome-Wide Analysis of ChREBP Binding Sites on Male Mouse Liver and White Adipose Chromatin. *Endocrinology* 156, 1982-1994.

Schmider, A.B., Vaught M., Bauer, N.C., Elliott, H.L., Godin, M.D., Ellis, G.E., Nigrovic, P.A. and Soberman, R.J. (2019). The organization of leukotriene biosynthesis on the nuclear envelope revealed by single molecule localization microscopy and computational analyses. *PlosOne Accepted and in press*.

Shah, A., Xia, L., Masson, E.A., Gui, C., Momen, A., Shikatani, E.A., Husain, M., Quaggin, S., John, R., and Fantus, I.G. (2015). Thioredoxin-Interacting Protein Deficiency Protects against Diabetic Nephropathy. *J Am Soc Nephrol* 26, 2963-2977.

Vokes, S.A., Ji, H., McCuine, S., Tenzen, T., Giles, S., Zhong, S., Longabaugh, W.J., Davidson, E.H., Wong, W.H., and McMahon, A.P. (2007). Genomic characterization of Gli-activator targets in sonic hedgehog-mediated neural patterning. *Development* 134, 1977-1989.

Yoshioka, J., Imahashi, K., Gabel, S.A., Chutkow, W.A., Burds, A.A., Gannon, J., Schulze, P.C., MacGillivray, C., London, R.E., Murphy, E., *et al.* (2007). Targeted deletion of thioredoxin-interacting protein regulates cardiac dysfunction in response to pressure overload. *Circ Res* 101, 1328-1338.